UC Riverside

UC Riverside Electronic Theses and Dissertations

Title

Synthesis and Characterization of Earth Abundant and Nontoxic Metal Chalcogenides Produced via Aerosol Spray Pyrolysis for Photovoltaic Applications

Permalink

https://escholarship.org/uc/item/2030z1q1

Author

Davis, Patrick John

Publication Date

2013

Peer reviewed|Thesis/dissertation

eScholarship.org Powered by the California Digital Library
University of California

UNIVERSITY OF CALIFORNIA
RIVERSIDE

Synthesis and Characterization of Earth Abundant and Nontoxic Metal Chalcogenides Produced via Aerosol Spray Pyrolysis for Photovoltaic Applications

A Thesis submitted in partial satisfaction
of the requirements for the degree of

Master of Science

in

Mechanical Engineering

by

Patrick John Davis

August 2013

Thesis Committee:

Dr. Lorenzo Mangolini, Chairperson
Dr. Javier Garay
Dr. Guillermo Aguilar

Copyright by
Patrick John Davis
2013

The Thesis of Patrick John Davis is approved:

Committee Chairperson

University of California, Riverside

Acknowledgments

It is hard to imagine that two years can go by so quickly, but I feel that I have been very fortunate to have had so many great people to help me pass the time. From day one of my existence at UCR, my advisor, Dr. Lorenzo Mangolini, has been a beacon of knowledge and support. I am forever grateful for the numerous intellectual discussions, incredible lessons during lecture, troubleshooting days in the lab, and general support Dr. Mangolini has given me to allow me to be able to write this thesis. Secondly, my family and girlfriend have had an unwavering faith in me. Their love and support helped keep me going on even the most difficult of days, and I owe them a great deal of gratitude. Hopefully as I journey home to be closer to them I can return the support they have so graciously given. My friends and girlfriend have also kept my ever growing desire for enthusiasm and excitement at bay, humoring me on my many excursions to try one thing or another in exploring all that Southern California has had to offer.

Friends and coworkers have also helped me immensely in the lab as well. Ozgul Yasar-Inceoglu has given innumerous hours of her time to help me with SEM and EDS analysis. Dr. Vullev's laboratory group has been extremely generous in assisting with my UV-vis analysis studies. Dr. Ilkeun has given XPS assistance and thoughtful discussion. Dr. Mangolini has given countless hours in the black hole known as the TEM. Dr. Feng's group has helped in my understanding and troubleshooting of XRD. Finally, all of our laboratory team have also given great advice, leant helping hands, and been great friends with which to spend time over the course of these two years, making the lab a truly enjoyable place.

ABSTRACT OF THE THESIS

Synthesis and Characterization of Earth Abundant and Nontoxic Metal Chalcogenides Produced via Aerosol Spray Pyrolysis for Photovoltaic Applications

by

Patrick John Davis

Master of Science, Graduate Program in Mechanical Engineering
University of California, Riverside, August 2013
Dr. Lorenzo Mangolini, Chairperson

A novel synthesis technique for the production of copper zinc tin sulfide (CZTS) nanocrystals has been developed using aerosol spray pyrolysis. CZTS is a quaternary semiconducting material that shows promise as a replacement to common semiconductors such as CdTe and CIGS for use in photovoltaic devices. CIGS is currently being commercialized in the photovoltaic industry, but rare and expensive indium and gallium components threaten its long term viability. CZTS looks to be one of the best alternatives to CIGS with all earth abundant and non-toxic materials and recent impressive gains in efficiency. A number of synthesis techniques have been thoroughly studied and detailed previously. In our novel approach, we synthesis single phase nanocrystals, starting with zinc, copper, and tin diethyldithiocarbamate precursors in a toluene solvent. The precursor solution is aerosolized using an ultrasonic nebulizer wherein the droplets are vacuumed through a tube furnace and nucleation occurs. We reproducibly synthesize kesterite, Cu_2ZnSnS_4, nanocrystals. This technique continuously

converts the chemical precursor into high-purity nanopowder with a production rate of ~50 mg/hour for an un-optimized, lab-scale reactor. Using the same precursor chemistry, we have also been able to deposit high-quality CZTS thin films directly onto Mo-coated Swiss glass substrates using the aerosol spray pyrolysis technique. A thorough discussion of the current photovoltaic field, the processing parameters and challenges of nanocrystal and thin film production, and the experimental results will be presented. Characterization via Raman spectroscopy, EDS, XRD, TEM and XPS will be offered along with future recommendations and considerations.

Table of Contents

Chapter 1 Introduction…….....……..**1**

1.1 Thesis Direction…….....……..5

Chapter 2 Motivation and Background…….....**6**

2.1 Background…….....6

2.2 Motivation and Literature Review …….....11

Chapter 3 Experimental …….....**18**

3.1 Precursor Synthesis…….....19

3.1.1 Copper Diethydithiocarbamate …….....19

3.1.2 Tin Diethyldithiocarbamate…….....20

3.2 Copper Sulfide (Cu_2S) Synthesis…….....21

3.3 Zinc Sulfide (ZnS) Synthesis…….....24

3.4 Tin Sulfide (SnS or SnS_2) Synthesis…….....24

3.5 Copper Zinc Tin Sulfide (CZTS) Synthesis…….....25

3.5.1 CZTS Nanocrystal Production…….....25

3.5.2 Thin Film Growth…….....26

Chapter 4 Results and Discussion…….....**28**

4.1 Zinc Sulfide…….....28

4.2 Copper Sulfide…….....31

4.2.1 Device Dependence…….....38

4.3 Tin Sulfide…….....40

4.4 Copper Zinc Tin Sulfide Results and Discussion…….....41

4.4.1 CZTS Nanoparticle Production…….41

4.4.1.1 Temperature Variation……..…….....48

4.4.1.2 Role of Zinc and Copper in CZTS Light Absorbing Material …….....49

4.4.1.3 Aerosol Variation and Powder Production ……...51

4.4.2 Thin Film Results and Discussion……52

4.4.3 Preliminary Annealing and Concentration Variation Experiments……..59

Chapter 5 Conclusion and Recommendations…….**.....61**

References…….....…….....…….....…….....…….....…….....…….....…….....…….**...63**

List of Figures

1. Energy Consumption Trends.....1
2. Renewable Energy Sources Breakdown.....2
3. California concentrated solar thermal energy collection.....3
4. Photovoltaic Material Prices vs Abundance.....8
5. Prospective layers of CZTS Solar Cell.....9
6. CZTS Efficiency Trends since introduction.....10
7. Annealing schematic use with first CZTS solar cell production.....13
8. Electron beam evaporation schematic.....14
9. Ion Sputtering Setup.....15
10. Thin Film Produced via sputtering technique.....16
11. Experimental apparatus schematic.....21
12. Three nebulizers used in synthesis.....23
13. Filling device for ultrasonic nebulizer.....25
14. Thin film experimental apparatus.....26
15. XRD of ZnS powder vs ICSD Standard.....28
16. ZnS formation chemical equation.....29
17. ZnS TEM.....30
18. Cu_2S TEM.....31
19. Particle Size variation Cu_2S.....32
20. Particle Size vs Precursor Concentration for Cu_2S.....33

21. Temperature vs Phase graph for Cu_2S.....35

22. XRD of Cu_2S vs ICSD standard.....36

23. Cu_2S Absorption Spectrum.....37

24. SnS TEM.....40

25. CZTS XRD.....42

26. CZTS Raman Spectroscopy.....43

27. CZTS EDS Analysis.....44

28. CZTS XPS Analysis.....45

29. CZTS TEM Images.....46

30. CZTS Absorption Spectrum.....47

31. CZTS EDS analysis Temperature vs Composition.....48

32. CZTS Crystal Structures.....50

33. Ultrasonic Nebulizer.....51

34. CZTS Thin Film SEM Images.....52

35. CZTS Thin Film XRD.....53

36. CZTS Thin Film XPS Sputtering.....54

37. CZTS Thin Film XPS vs EDS Film Composition.....55

38. CZTS Thin Film Raman Spectroscopy.....56

39. CZTS Thin Film UV-vis Absorption Spectrum.....57

40. CZTS Thin Film Cross Section image.....58

41. CZTS Thin Film initial Annealing Results from EDS.....59

42. CZTS Thin Film initial precursor concentration changes affect morphology.....60

1. INTRODUCTION

According to the Department of Energy, the United States' appetite for energy consumption is on a continually increasing trajectory [1]. This energy consumption has a number of unfortunate effects to the environment. Specifically, 56% of our energy comes from carbon dioxide emitting energy sources, as can be seen in Figure 1 [1]. The countries that make up the United Nations all recently signed an agreement that if the average temperature of the earth rises by 1.6 ℃ above its current temperature, the world

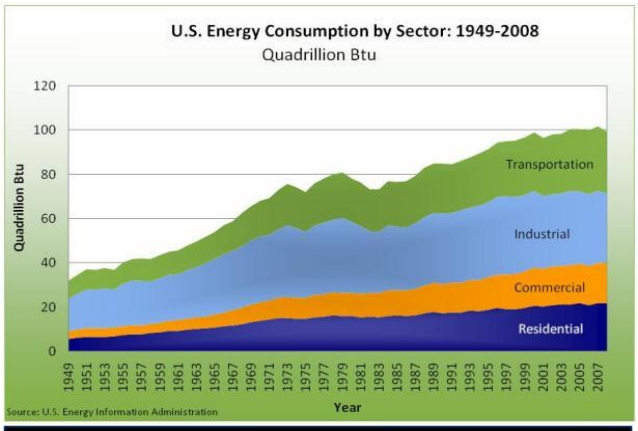

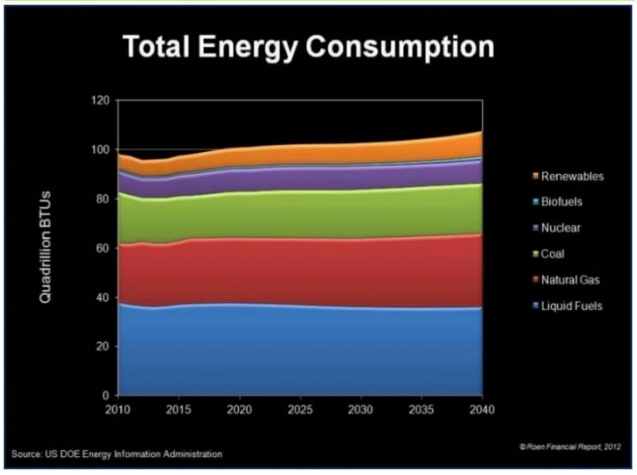

Figure 1a. U.S. Energy Consumption by Sector: 1949-2008.

Figure 1a shows the trend over the last 50 years of the United States' incredible demand for energy increasing. Recently, energy demand has decreased slightly compared to previous peaks in 2007, but the DOE still predicts increasing consumption trends to continue well into the next decades as seen in Figure 2b.

Figure 1b. Total Energy Consumption Predicted Trends over the next 40 years.

Figure 1b represents the predicted quadrillion BTUs of consumption expected of each energy type. Although the DOE does expect Renewable Energy levels to increase, the field expects and hopes that it contributes a much larger contribution than is depicted.

Figure 1a and 1b from [2]

is going to be in serious trouble [2]. Carbon dioxide levels have been scientifically shown to be related to increasing temperatures and some 97% of climate scientists in a recent

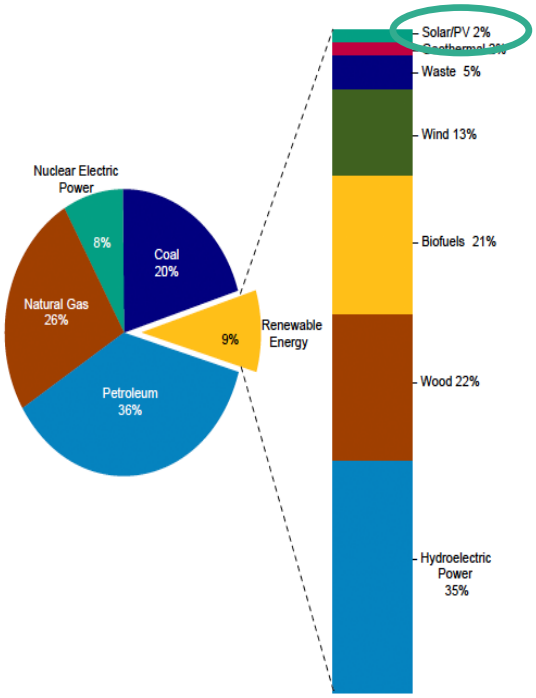

Figure 2. Energy production from each major source. Clearly renewable energy has a lot of room for growth, and solar energy has an even greater potential. It currently supplies merely 0.2% of the United States' energy. Nevertheless, the EIA shed light on the advancements the industry has been making. Claiming that, "Although solar energy contributed relatively little in terms of the absolute increase in total renewable energy consumption in 2010, solar energy use exhibited the highest rate of growth of all the renewable fuel categories" [1].

Figure from [1]

study agree that global warming is due to human effects, specifically stating that it is "very likely that anthropogenic greenhouse gases have been responsible for most of the unequivocal warming of the Earth's average global temperature in the second half of the twentieth century" [3]. Unless we can change our habits, the world may not be useful in the way in which we use it today for much longer. In 2011, only 9% of our energy consumption in the United States was from renewable energy sources [1]. Many of these sources include hydroelectric, biomass, wind, and solar energy. Unfortunately, only 2% of the renewable energy came from solar energy [1].

This is startling given that about 10,000 times the amount of energy consumed each day worldwide strikes the earth in that same day. [4]. Solar energy has garnered much attention recently both in the political and scientific world. Politically, many states

have begun incentive programs to encourage solar panel installation on homes and businesses. Scientifically, the Department of Energy, National Science Foundation, and many other government and grant foundations have contributed to research projects as well as new solar power plants. Most recently, with major loan funding from the Department of Energy, a large power generation system using solar thermal energy has been constructed in the Mojave Desert in California. This setup uses solar panels to focus

Figure 3 shows a large concentrated solar thermal energy collection setup. Three of these setups currently reside in the California Mojave Desert [4].

Figure from [5]

light onto a boiler which in turn acts as a steam generator to produce electrical energy from mechanical work [6]. Although progress is being made within the field, clearly the industry still has an immense potential for growth that is yet untapped.

One of the reasons for this untapped potential is, as many would expect, cost. Solar energy in its current state depends on a number of materials that are expensive to obtain and dangerous to handle. Solar thermal energy is currently the most efficient means to garner sunlight's energy and turn it into electricity. California currently has a large investment into solar thermal farms in the desert. Unfortunately, this very efficient means of harnessing solar energy, requires huge investments, both monetary and spatially. Thus, it is not a viable option for everyday uses such as residential home

application. A means that could transfer the energy of the sun directly into electrical energy without moving parts is thus in high demand.

A device that does just that, is called a photovoltaic device. It directly converts photons of desired energies into an electrical current. Silicon was the first material to be used in photovoltaic devices when it was introduced in 1954 [7]. Such a product that could convert the sun's energy into electrical energy could be used throughout the world. In order for such a device to be a viable alternative form of energy, a number of things must be possible, however. It must be able to be affordable, even though we think of gas and electricity to be extremely expensive in their current states, they have hundreds of years of advancement that has brought their costs to be low enough that even with free energy from the sun the cost of solar energy cannot yet compete directly with that of coal and natural gas [8]. It must also be easily produced in very large numbers. If we are to make this an actual alternative, it is going to need to be mass produced with materials that have no shortages or large price variances in short amounts of time. If this device is going to be used by a great number of people and produced by just as many, it also must be a material that is both safe to handle and safe to own. All of these considerations have helped push Copper Zinc Tin Sulfide (CZTS) into the forefront of the photovoltaic industry today.

Thesis Direction

This thesis will discuss the motivations behind producing photovoltoaic devices, the current state of the technology, and then delve into the material of interest, CZTS and why it is a viable alternative for the current market and a great prospect for the future of the industry. The roadmap to producing CZTS, as well as the current production status will be discussed. Chapter four will discuss the interesting results of our current research and the advantages of our process and understanding of the material we produce. Finally, concluding remarks and future direction will be given.

2. MOTIVATION AND BACKGROUND

2.1 Background

Given all of these demands that must be met in order to satisfy the need for a solar energy field, silicon has been the major material of choice for the photovoltaic device even to this day. In 1954, Silicon was first shown to be a possible material to turn sunlight into useful electrical energy when Daryl Chapin, Calvin Fuller, and Gerald Pearson create the first photovoltaic device in the United States using silicon [7]. In such a device, photons with an energy of at least the band gap energy, typically around 1.5eV are absorbed onto a material with either a large amount of electrons in its valence band that it can donate, called an n-type semi-conductor, or a large amount of holes for which electrons can be accepted, called a p-type semiconuctor [9]. If the photon has energy in the range of the material's band gap energy, then it is absorbed by the material and its energy excites an electron into the conduction bad where it will fill a hole in the n-type semiconductor. Once a current can be made, then electrical contact is made so that the electrons will be pulled to the anode and holes will be accumulated at the cathode [9]. Then, you have a photovoltaic device which can transfer this electrical energy into the grid. Although in 1954, this silicon devices efficiency was merely 4%, today the best silicon photovoltaic device achieves >25% efficiency [7,10].

Silicon's efficiency gains are important because it is still the most commonly used material in the photovoltaic industry. Nevertheless, it is also one of the most commonly used materials throughout the electronics industry. Silicon makes an excellent semiconductor and thus it is used in nearly everything that can function with a

semiconductor. Scientifically speaking, silicon's theoretical maximum efficiency is also merely 29% which current research is already approaching [10]. A major problem with silicon, however, is that it has a relatively small absorption coefficient due to it being an indirect band gap semiconductor. The small absorption coefficient requires absorption layers of around 100 micrometers, orders of magnitude greater than those that can be developed using other direct band gap materials [11]. Silicon is earth's second most abundant material [12], but its continued demand, theoretical efficiency limits, special demands, and processing concerns threaten the long term viability of a silicon based photovoltaic industry. The necessarily thick layer needed to produce photovoltaic devices using silicon, also pose future challenges as the industry continually readies smaller devices that can be used in a variety of ways and locations.

Scientists have begun to explore what lies beyond silicon for the photovoltaic future. Although many materials have been researched and considered, two of the most common replacements have been Cadmium Tellurium (CdTe) and Copper Indium Gallium Sulfide (CIGS). Both of these semiconductors are now reaching commercial production levels, and companies such as First Solar have begun producing them as replacements for silicon semiconductors in the photovoltaic industry [13]. Cadmium tellurium and CIGS both have a theoretical efficiency limit of roughly 30% based on the Shockley-Queisser limit [14,15]. In commercial grade products they are expected to be mass produced at the 10% efficiency level, proving to be viable alternatives to the current silicon status quo.

When developing such products, however, serious concerns exist as to the future viability of devices using these materials. If the photovoltaic industry wishes to be plausible as a large scale energy sector, it must have product with materials that are safe, inexpensive and attainable for the foreseeable future. According to OSHA, Cadmium is considered a human carcinogen, and thus its production and handling adds considerable cost and cautionary measures [16]. Thus, Cadmium Tellurium does not seem to be a material that could be considered for large scale production in the long term. Cadmium is also used with CIGS as an n-type semiconductor layer. CIGS also uses indium which is an extremely expensive material with its cost ever increasing [17].

Due to these financial and safety concerns, neither of these materials seem capable of bringing the photovoltaic industry into the mainstay of the world's energy market. Over the last 25 years, researchers have begun considering a material that is not only earth abundant but also environmentally friendly and safe. Copper Zinc Tin Sulfide (CZTS), has garnered significant attention in this

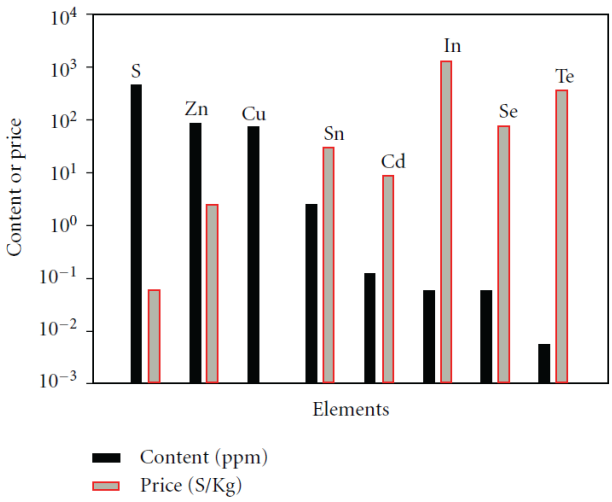

Figure 4 expresses the average content abundance as compared to the current price of each element. Clearly, cadmium, indium, selenium, and telerium represent expensive semiconducting materials. Although tin appears to be on a similar level, its abundance is much greater than any of the aforementioned materials, which is a key factor in the prospective future of this technology.

Figure from [17]

regard. Figure 4 shows the abundance and cost of the major materials currently used for photovoltaic devices. Clearly it can be seen that CZTS uses significantly more abundant and less expensive materials. Since its introduction in 1997 with a thin film photovoltaic device with an efficiency of merely .66%, CZTS has quickly made significant advances in its efficiency as can be seen in Figure 6 [18]. Many companies, including IBM and Dupont, have put considerable investments into producing and developing CZTS photovoltaic devices. This is because CZTS could be used to make a solar cell out of all abundant, nontoxic elements as seen in Figure 5.

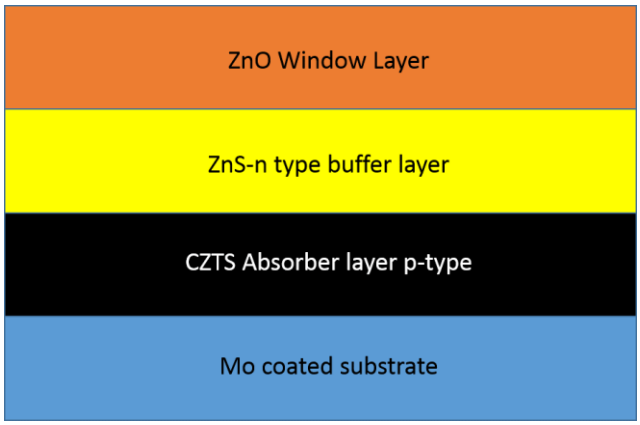

Figure 5. Possible layers of an earth abundant, non-toxic CZTS solar cell.

Mo-coated glass substrate with CZTS p-type semiconductor light absorber layer, ZnS n-type semiconductor buffer layer, and then a typical ZnO window layer.

CZTS is a p-type semiconductor, and as a photovoltaic device it has a theoretical efficiency limit of 32.2% [21]. Thus, it is a very viable material for the future of the industry. It is a quadernary chalcogenide typically produced in kesterite phase in current research [22]. It has a band gap of between 1.0-1.5 eV, and it has a large absorption coefficient of 10^4 cm^{-1}[22]. Advances in the industry have brought its current efficiency up to a maximum of 11% as developed by IBM using a selenium/sulfur substitute to gain efficiency [19]. One of the current challenges with CZTS, however, is that there is no

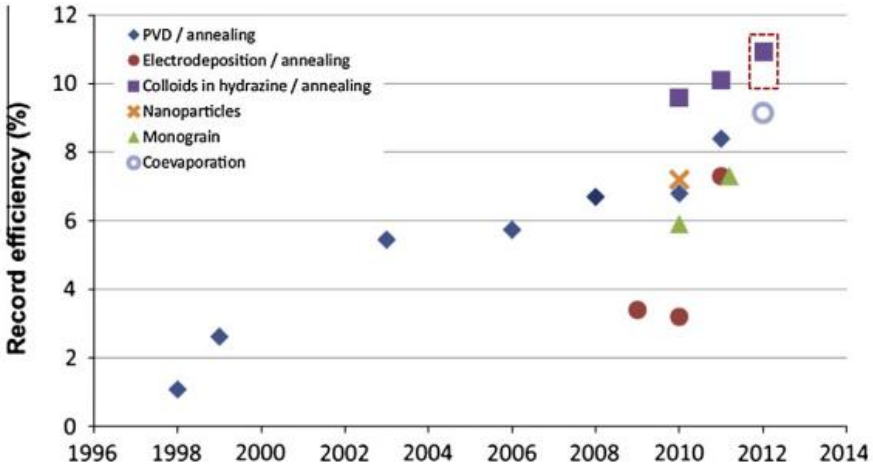

Figure 6. CZTS efficiency trends since its introduction. Current efficiency levels have reached 11% in IBM laboratories led by Todorov [19].

Figure from [20,21]

agreed upon method to synthesize this semiconducting material. CZTS can be synthesized using vacuum, non-vacuum, thin film, and nanocrystal production processes. The majority of the synthesis methods involve depositing the CZTS material onto a substrate as a thin film, but it is also possible to produce CZTS nanocrystals. Both methods will be studied herein. A variety of synthesis techniques exist due to the common existence of multiple phases and common compound impurities such as Cu_2S, thus these methods all attempt to find a new way to make phase pure CZTS [23].

2.2 Motivation and Literature Review

IBM has invested significant amounts of money in the hopes of bringing CZTS photovoltaic devices to the forefront of the commercial market. With such vast resources, they are considered to be at the top of the field with their most recent 11% record efficiency CZTS device [19]. IBM previously, as well as others including papers by references [23-25], use a synthesis method that involves using a hydrazine solution based process. Although hydrazine is a very dangerous, toxic material to work with, many have had similar success in producing phase pure, efficient CZTS [19, 23-25]. In this process, the individual materials are spin coated onto a molybdenum coated soda lime glass substrate. After the constituents are deposited, the substrate and material are annealed at temperatures greater than 500℃ in a sulfur environment [19]. The process to develop the materials before spin coating, however, has major challenges for the safety and delicate processing environment necessary to use this method due to the hydrazine.

Todorov and his team of scientists have been major players in the efficiency gains of CZTS, working in IBM laboratories, they have developed the hydrazine ink processing method, and it currently holds the record for highest efficiency, using a selenium sulfur complex [19]. In this process all of the metal chalcogenides are dissolved into a hydrazine solution individually and then mixed together. Two different precursor solutions are made from this process. A slurry consisting of those materials that are not soluble in hydrazine and thus form a nearly homogenous mixture is one of the components, while another solution consists of those materials that are soluble in hydrazine [19]. These two are then placed onto a centrifuge and applied to molybdenum

coated soda lime glass. Some of the materials are simply dried on the substrate, while others require a higher temperature annealing setup. In the end, however, they show that a high energy yield thin film photovoltaic cell can be produced using this method [26].

One of the main advantages to this process, is that it appears that few if any impurities are formed in the final product. Currently, a major challenge in producing CZTS is the existence of ZnS, CuS, and SnS impurity components in the material. ZnS is especially challenging because its XRD peaks are nearly identical to those of phase pure CZTS [27]. In their recent publication, "Reaction pathways for the formation of $Cu_2ZnSn(Se,S)_4$ absorber materials from liquid-phase hydrazine-based precursor inks," W. C. Hsu, B. Bob, W. Yang, et al explain the process by which phase pure CZTS nanocrsystals can be produced [28]. In their process, they believe the impurities are eliminated when they make a slurry and a solution of materials as precursors in hydrazine. By creating these hydrazine mixtures, they believe the intermediate phase impurities become ineligible to be produced in their layered substrate setup [19, 28].

The challenges of this process, though, exist in its lengthy processing time, greater than 1 week according to the authors in [28], which could prove inefficient in a large scale setup. Although it is stated that this process exists in room temperature and non-vacuum environments, great precautions still exist due to the handling and use of hydrazine in the major steps of this synthesis [19,23-25,28]. Hydrazine is a toxic, dangerous material. To make these efficiency gains, selenium has also been used along with sulfur, but once again this poses a problem to the idea of using non-toxic earth abundant materials for future solar cells. Although selenium is not as dangerous as many

rare earth elements, it is toxic when exposed to in high concentrations, and it is also a very costly material on the same level as Tellerium, which stands to deteriorate some of the major advantages of CZTS being a non-toxic earth abundant and affordable solar cell material [17, 29].

In 1997, H. Katagiri, N. Sasaguchi, S. Hando, et al. published "Preparation and evaluation of Cu_2ZnSnS_4 thin films by sulfurization of E-B evaporated precursors" [18]. They proposed using an electron beam vapor deposition method to produce layers of a

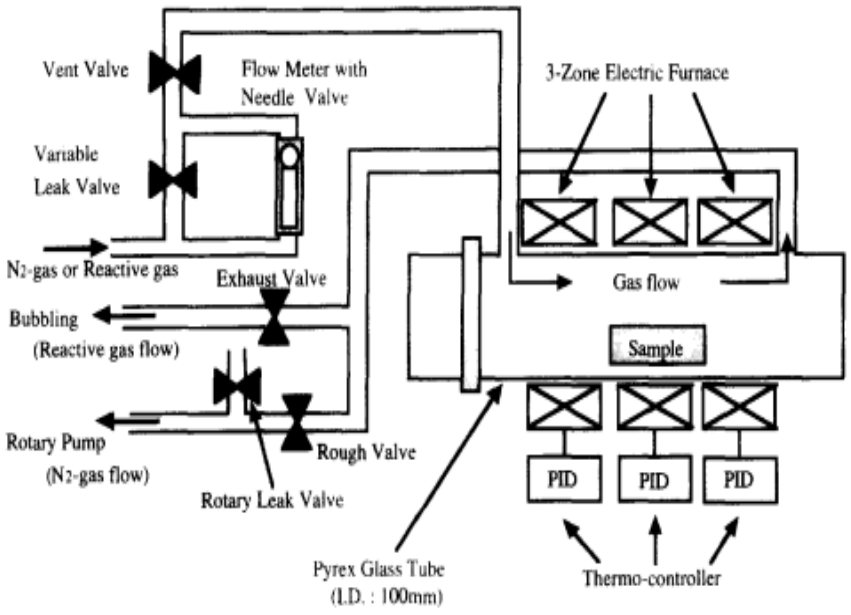

Figure 7 shows the original annealing setup for sulfurization in H. Katagiri's first ever CZTS thin films. This original setup was complex and proved to incapable of creating a high vacuum environment to properly eliminate impurities in the final film.

Figure from [18]

light absorbing CZTS thin film solar cell [18]. Similar to a sputtering technique, a target precursor is barraged with electrons causing it to quickly become a vapor and deposit

itself onto the above soda lime glass (SLG) substrate which was heated to 150℃ [18]. This was done individually with each precursor. First a 1600 angstrom layer of zinc was deposited, followed by a 2300 angstrom tin layer, and finally a copper layer 1800 angstroms thick was deposited. These thicknesses were based on atomic weight ratios and densities desired for stoichiometric CZTS. As in many thin film deposition techniques, a second phase of synthesis involves adding the needed sulfur into the layered film. A schematic of H. Katagiri's annealing setup can be seen in figure 7. Nitrogen and

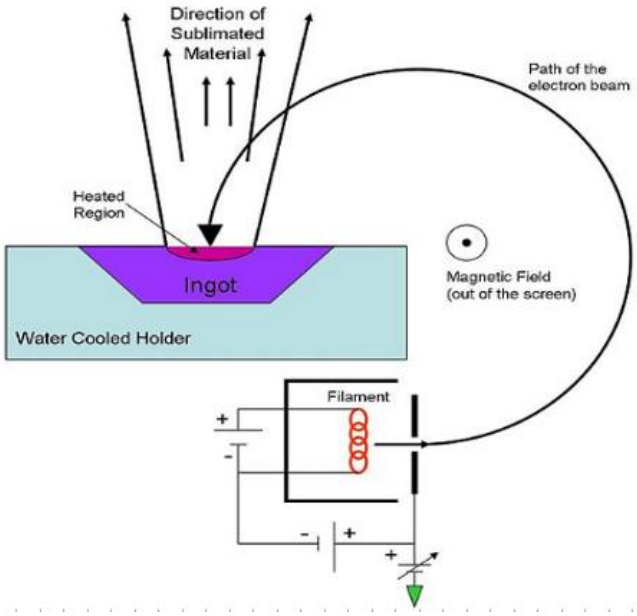

Figure 8 depicts an electron beam evaporation system for depositing precursors onto desired substrates. In this scenario, a substrate would typical be directly in the pathway of the sublimated material.

Figure from [31]

hydrogen sulfate gas were flown through a quartz tube with the sample and heated to 500℃. This device was able to produce a solar cell with a conversion efficiency of .66% using a cell with layers set up as Al/ZnO/CdS/CZTS [18]. H. Katagiri has published a number of papers thereafter tuning this process. In 2003, he found that changing the first layer of precursors to a zinc sulfide layer instead of just zinc and varying its thickness allowed a variation in the stoichiometry of the final cell [29]. A new method of sulfurization used higher vacuum to create a better more stable cell as well. He was even

able to increase his efficiency by an order of magnitude to 6.7% recently [30]. Overall, H. Katagiri has remained a strong figure in the production of CZTS solar cells, more recently focusing on the sulfurization method and its role in the efficiency of the overall cell [30].

Similar to electron beam evaporation, is the sputtering deposition method as seen in figure 9. Instead of using electrons, ionic gas molecules bombard a sputtering target which is thus given an energy higher than its binding energy, forcing its atoms to escape and bind with the substrate surface as shown in figure 9.

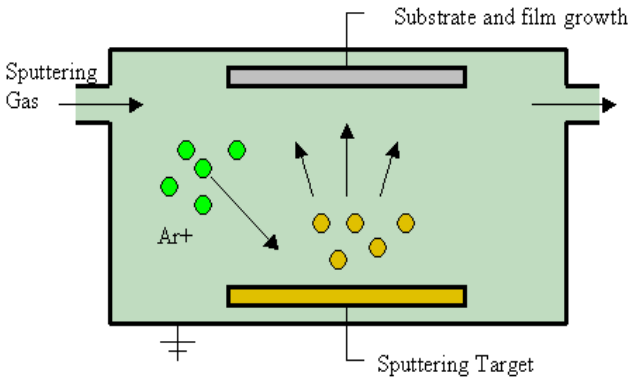

Figure 9. General sputtering setup using Argon as a sputtering gas. The three sputtering targets all had different sputtering powers due to the different binding energies of the target precursors [32].

A. Khalkar, K-S Lim, S-M Yu, et al have developed a co-sputtering technique where a radio frequency magnetron system sputters Cu, ZnS and SnS targets onto a soda lime glass substrate simultaneously under a high vacuum environment [33]. In their study, they were able to grow a thin film by simultaneously sputtering all three precursors onto a soda lime glass substrate. Nevertheless, impurities and secondary phases were found to exist in the film, and as is common for vacuum based deposition methods, a secondary annealing step was necessary. The group studied the effectiveness of sulfur environments for annealing and found that it was much more beneficial to use solid sulfur

and vaporize it inside of a tube furnace at atmospheric pressure to add sulfur and remove any impurities from their samples. Similar to others [33-35], they found that annealing at 530°C for 10 minutes under this environment was ideal [33]. Figure 10 shows a thin film produced via the co-sputtering technique after annealing. This group was able to use this method to produce a CZTS thin film with the ideal kesterite structure with a band gap of 1.5 eV and an optical absorption of 1.1 x 10^4 cm^{-1} showing that this is indeed a viable synthesis method [33]. Challenges with a postannealing step and the high energy constraints of the sputtering setup worry many about the scalability of such a process, however.

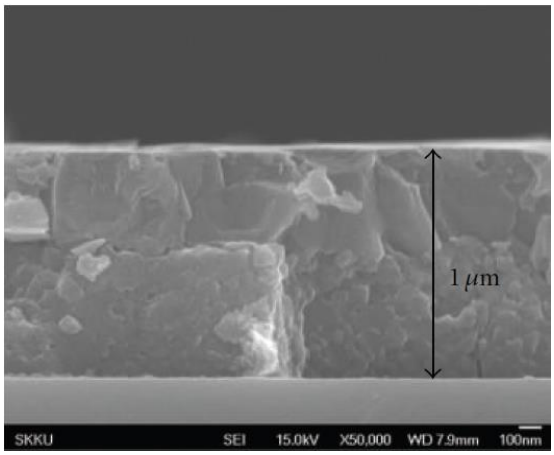

Figure 10 shows a thin film produced via co sputtering of Cu, ZnS, and SnS precursors simultaneously. Large grain growth and uniform film thickness are exemplary.

Figure from [33]

Another major method of synthesis involves using wet chemistry techniques to make batch solutions of CZTS precipitated nanocrystals. A number of studies have shown this method to be plausible using a variety of solvents [28,34,36]. C. Steinhagen, et. al, have shown that they can synthesis CZTS nanocrystals with a mixture of copper acetylacetonate, zinc acetate dihydrate, tin chloride, and elemental sulfur in a solvent of oleylamine [36]. The solution is degassed, purged, and then heated to 280°C. After the mixture is complete, ethanol is added to form the CZTS precipitate after the mixture has

cooled, and the precipitate is removed and further purified in chloroform. C. Steinhagen et al, have found they are able to make kesterite phase, slightly sulfur deficient CZTS nanocrystals with particle size around 10nm for use in photovoltaic devices. H. Yang, et al, have replicated this experiment and found the nanoparticles are also of great interest in the thermoelectrics industry, where they were able to produce thermoelectric devices from the as synthesized CZTS nanocrystals [28].

Similar to studies of Steinberg and Yang, S.W. Shin et al. have produced CZTS nanocrystals in a wurtzite phase using an adaptation of the precipitated solution method. An aqueous synthesis method involves suspending the aforementioned particles in deionized, high purity water, heating, and centrifuging to remove said nanoparticles. It is also stated that the final product, wurtzite CZTS nanocrystals, is soluble in deionized water [34].

Finally, a method we are significantly interested in is that of using spray pyrolysis to produce CZTS. Although the authors in [37] have produced thin films using ultrasonic spray pyrolysis, our method varies greatly, both in growing our thin films as well as producing nanocrystals. They use different precursors, specifically an aqueous solution of cuprous chloride, zinc acetate, and stannic chloride all dissolved in a thieoreau solvent and have only focused on thin film growth. As the authors in [38] have stated, nanocrystals have great promise in CZTS production when it comes to scalability. Instead of having to make a single layer of one solar cell at a time with thin film growth, nanocrystals allow a printable ink to be used in batch production of much larger scales. These inks could be used to coat a variety of substrates for different uses, and allow the

material to be cheaply produced in large quantities for fast and inexpensive production. For these reasons, we have studied the synthesis of aerosol spray pyrolysis to create nanoparticle CZTS. Thin film growth has also shown promise with our method, and it still shows great promise in the photovoltaics industry for research and development purposes. Even with the great variety of processing methods already available, synthesis of CZTS for use in photovoltaics continues to be a significant area of interest in the photovoltaic industry and we hope to contribute a method that will further the field toward becoming a viable option and competitor to CIGS solar cell technology with affordable and simple production with few dangerous or expensive components.

3. EXPERIMENTAL

As has been described by H. Yang in [28], there are significant advantages to using a nanocrystals developed material to make photovoltaic devices instead of having to make one device at a time as is common with many thin film procedures mentioned above. In order to develop a technique to produce bulk material of CZTS nanoparticles, we first set out to produce Copper Sulfide (Cu_2S), Zinc Sulfide (ZnS), and Tin Suflide (SnS or SnS_2) with our desired experimental setup to learn from and explore the ideal conditions with which to produce CZTS.

3.1 Precursor Synthesis

Precursors to the following synthesis included copper diethyldithiocarbamate [$Cu(dedc)_2$], zinc diethyldithiocarbamate [$Zn(dedc)_2$], and tin diethyldithiocarbamate [$Sn(dedc)_4$]. The zinc complex was purchased from Sigma-Aldrich (97%). Similarly, all constituent chemicals were purchased from Sigma-Aldrich. The copper and tin precursors were synthesized using wet chemistry techniques described by A. Khare, A. Wills, L. Ammerman, et al in the supporting materials of "Size Control and Quantum Confinement in Cu_2ZnSnS_4 Nanocrystals" [38]. To ensure safety, all processing was done inside of a fume hood.

3.1.1 Copper Diethyldithiocarbamate

To synthesize copper diethyldithiocarbamate, 10.85 grams of sodium diethyldithiocarbamate dissolved in 300ml of reagent ethanol was added dropwise to a solution composed of 4.03 grams of copper (II) chloride dissolved in 100 ml of reagent ethanol with constant stirring. The black precipitate that forms is collected via filtering

and washed four times using excess reagent grade ethanol followed by four rounds of washing with deionized water. The black powder was dried under vacuum with slight heating at 50°C overnight.

3.1.2 Tin Diethyldithiocarbamate

Tin diethyldithiocarbamate was similarly synthesized. 27 grams of sodium diethyldithiocarbamate was added to 300 ml of ethyl alcohol. Precautions were necessary to create the solution of tin (IV) choride, however, due to the reactivity of tin (IV) chloride in the presence of oxygen. To ensure safety, 2 milliliters of liquid tin (IV) chloride was added to 300 ml of ethyl alcohol via a Schlenk line with induced flow due to vacuum. The sodium solution was added dropwise to the tin solution with constant stirring. An orange precipitate is formed and collected via filtering. The precipitate is then washed four times with ethyl alcohol followed by four times washing with deionized water and dried under vacuum and 50°C overnight [38].

3.2 Copper Sulfide (Cu_2S) Synthesis

The process, described in our recent publication in MRS Communications Research Letters, "Single precursor synthesis of copper sulfide nanocrystals using aerosol spray pyrolysis," uses an experimental apparatus as shown in Figure 11 [39]. A single source precursor of $Cu(dedc)_2$ in toluene has typical concentration of 4-6 mg/ml. A nebulizing device creates an aerosol of the precursor which is aerodynamically dragged through a heated tube furnace and collected via filtering before the vacuum pump. Three devices were found to be capable of producing the desired aerosol to produce copper sulfide. These devices included a an ultrasonic nebulizer from Sonaer Ultrasonics, a single jet Collison-type atomizer from BGI, and an Iwata Eclipse HP-BCS airbrush spray system typically used for spray painting. All of these devices did require flow gases for them to function ideally, however, with the ultrasonic nebulizer requiring a flow gas only to help move the aerosol created into the in line system from its position in the nebulizer. The

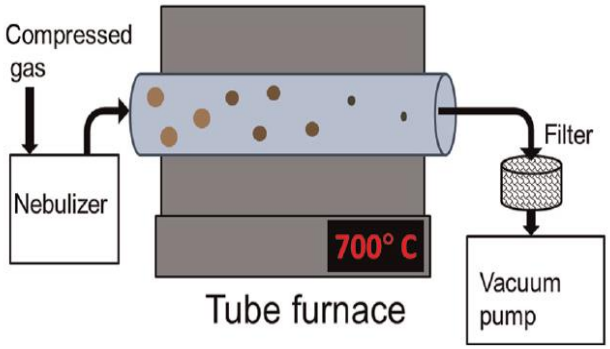

Figure 11. Aerosol spray pyrolysis setup. Nitrogen gas flows through the single jet collison type atomizer creating a venturi. The $Cu(dedc)_2$ precursor, in toluene, becomes an aerosol droplet as it exits the jet atomizer. It is carried through the tube furnace, a standard 1 foot tube furnace where a typical temperature of 500℃ evaporates our solvent, decomposes the precursor and creates copper sulfide. Upon exiting the furnace the nanoparticles are captured on a stainless steel mesh filter**.**

Figure from [39]

Collison-type jet atomizer required a flow pressure of roughly 30 psi, flowing around 10scfh of nitrogen to produce an aerosol. Finally, the airbrush likewise required around 15 scfh of nitrogen gas flow at a pressure of around 35-40psi to produce an aerosol. Based on previous experimental studies and the manufacturer's specifications, average droplet size for the ultrasonic nebulizer and the jet atomizer were roughly 2.2 micrometers in diameter, while the industrial grade airbrush creates larger particles of around 5-10 micrometers [40].

Once the aerosol was created in one of the nebulizers, it was aerodynamically dragged into a 1" quartz tube and through a tube furnace. The tube furnace temperature ranged from 500-800°C depending on the desired phase we wished to produce. The hot region of the furnace is approximately 12" in length. Based on the flow velocity of our gases, we calculate the residence time in the furnace to be ~500ms, and vacuum inside of the system was kept steady at around 200 Torr. The copper sulfide nanocrystals were collected via a stainless steel mesh where a coated copper transmission electron microscope (TEM) grid could be attached to deposit the powder. The material could also be removed from the stainless steel filter to be analyzed as a powder using X-Ray Diffraction (XRD) or added to chloroform in dilute concentrations for UV-vis optical absorption analysis [39].

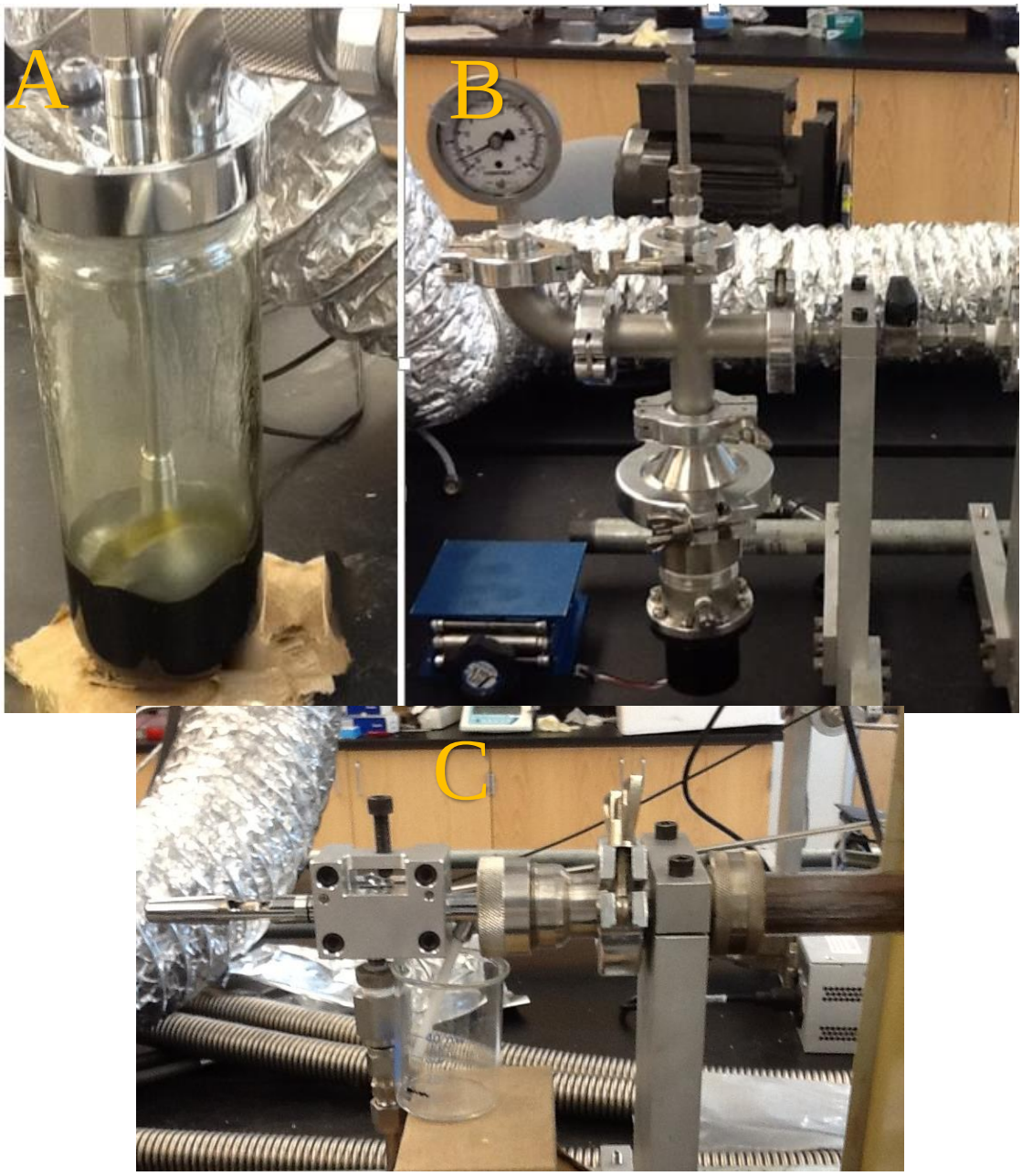

Figures 12a, b, c depict the three different nebulizers used independently throughout our experiments. 12a. is a BGI Collison type jet atomizer, 12b is an ultrasonic nebulizer, and 12c is an Iwata spray brush with a machined piece to control constant flow rates.

3.3 Zinc Sulfide (ZnS) Synthesis

Zinc Sulfide was synthesized using aerosol spray pyrolysis just as previously described. This synthesis technique was adapted from Swihart, et al in their publication [41]. Zinc precursor, zinc diethyldithiocarbamate purchased from Sigma-Adrich (97%) was typically dissolved in toluene in a ratio of 500 mg precursor for every 100 ml of toluene solvent. Zinc sulfide nanoparticles were typically created with a furnace temperature of 800°C. Due to the heightened temperature, the grey particles were collected farther down the setup, about 24 inches from the furnace, just before the vacuum pump, rather than merely 4-5 inches after the pump which was typically the case with copper sulfide synthesis. Run time varied, but ideally was around 25-28 minutes depending on the setup used. 20 milligrams of ZnS powder were routinely collected in this time.

3.4 Tin Sulfide (SnS) synthesis

Tin Sulfide was synthesized using aerosol spray pyrolysis as well. Nevertheless, SnS was only created using the ultrasonic nebulizer device seen in figure 12b. Typical tin diethyldithiocarbamate precursor concentration was 10mg per ml of toluene solvent. Temperature ranged from 600-800°C. Run time was similarly 25 minutes.

3.5 Copper Zinc Tin Sulfide Synthesis

3.5.1 CZTS Nanocrystal Production

Copper Zinc Tin Sulfide nanocrystals were synthesized using aerosol spray pyrolysis. The nebulizing device used was the ultrasonic nebulizer only as it showed the most reproducible results with all of the previous experiments. Copper diethyldithiocarbamate, tin diethyldithiocarbamate and zinc diethyldithiocarbamate precursors were dissolved in a toluene solvent all together. Based on desired stoichiometric molar ratios of Cu:Zn:Sn of 2:1:1, Cu:Zn:Sn ratios were 210mg:98mg:220mg respectively in 40ml of toluene. Solution was then sonicated using a sonicating device for roughly 25 minutes, to ensure proper dispersion and dissolution. In the ultrasonic nebulizer, an aerosol was formed with the complexes where it was carried by a pressure gradient and an argon gas flow of 750 sccm. Typical pressures were of the order of 25kPa absolute pressure. The aerosol travelled through the furnace with temperatures ranging from 650-800°C and collected using a similar stainless steel mesh at the exit of the furnace. Once again, the heating region was 12" in length and the calculated resonance time was still ~500ms. As shown in figure 13, a system to add precursor solution using a syringe without stopping the run has allowed us to obtain greater amounts of powder as compared

Figure 13. Experimental setup that extends run times to create much longer runs and thus greater amounts of powder per run.

to previous experiments. Run times range from 25-45 minutes. It appears we are able to make roughly 1mg/min of CZTS nanocrystals.

3.5.2 Thin Film Growth

CZTS was also synthesized using aerosol spray pyrolysis to grow a thin film on a molybdenum coated glass microscope slide. A schematic of this setup is shown in Figure 14. An ultrasonic nebulizer still created an aerosol which was transported via aerodynamic drag with an argon flow gas of 750 sccm. A device was constructed to hold a roughly 1cm^2 glass substrate about 8 inches from the aerosol source. This substrate was inside a 2" diameter quartz tube surrounded by a tube furnace. Temperatures were varied from 400-500°C. Run time was typically 25 minutes wherein the sample was left to cool inside the tube and furnace for roughly 30 minutes before removal. The setup is still kept at around 200 Torr vacuum levels. A picture of one of the films grown is in Figure 14 where we used a silicon oxide substrate originally.

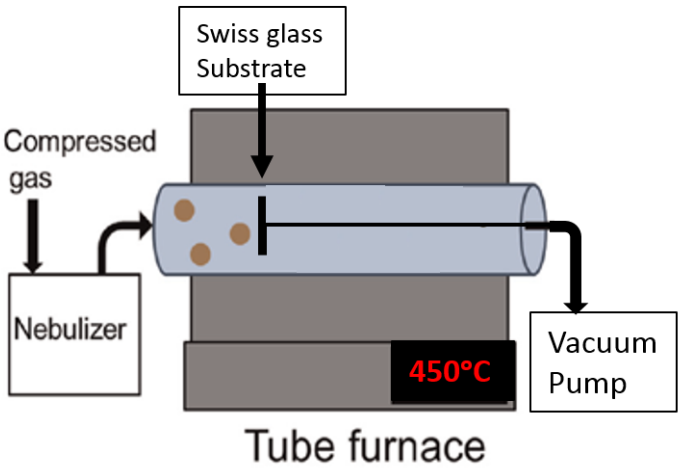

Figure 14. Similar to the schematic shown for our nanoparticle production setup, figure 14 represents the setup we use to grow thin films. Our ultrasonic nebulizer creates an aerosol while the compressed gas helps aerodynamically drag the droplets into a 2" quartz tube where they flow into the tube furnace. The furnace is typically run at 450°C. The substrate is suspended inside of the quartz tube. The nozzle to substrate distance is roughly 30cm.

Thin film growth of light absorbing materials onto given substrates to produce solar cells has been widely used throughout the research field. Ultrasonic spray pyrolysis has even been deployed to develop a CZTS absorption layer [42]. Nevertheless, given our success in producing nanoparticles, we attempted to develop a single source precursor method to deposit CZTS on thin film substrates to produce solar cells.

4. RESULTS AND DISCUSSION

4.1 Zinc Sulfide

Of the three constituents synthesized with our setup, Zinc Sulfide was the most reproducible. It was possible to produce ZnS nanoparticles using all three apparatuses, and particle size and phase control was tunable. Zinc sulfide shows strong promise in the semiconductor field of research, and many have even show that it can exist as an n-type layer in solar cells. Nevertheless, we wished to produce all three constituents of CZTS separately to ensure the process was compatible with our desired material goal.

Zinc sulfide particles were confirmed with X-Ray Diffraction using a k-alpha copper source with wavelength 1.5 angstrom and high resolution transmission electron microscopy (TEM). Particle size was found to be in the range of 15-20 nanometers. Almost exclusively we produced stoichiometric, cubic ZnS as characterized via XRD analysis. An Inorganic Crystal Structure Database (ICSD) standard in Figure 15 shows the agreement of our samples with the given standards.

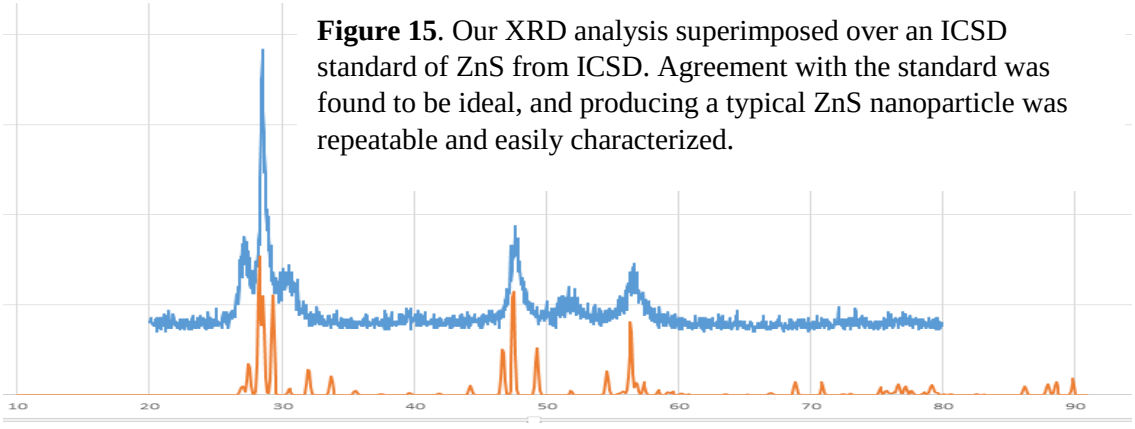

Figure 15. Our XRD analysis superimposed over an ICSD standard of ZnS from ICSD. Agreement with the standard was found to be ideal, and producing a typical ZnS nanoparticle was repeatable and easily characterized.

Although the process followed was very similar to that used by Swihart et. al. in our synthesis of Zinc Sulfide, we believe that because a diffusion dryer was not used in our system that our precursor does not enter into a vapor phase before reaching the furnace. Rather, an aerosol is produced via the jet atomizer with nitrogen flow gas, wherein it enters the furnace [41]. At this time, the droplet vaporizes and nucleation occurs in a mechanism as shown by Figure 16. In the furnace the ZnS particle is formed and collected via stainless steel mesh filtering as discussed.

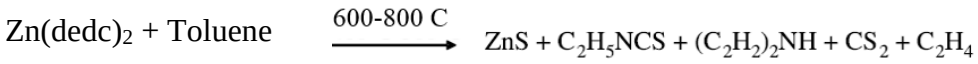

Figure 16. Chemical process by which Zinc diethyldithiocarbamate becomes ZnS [43].

Figure 17 further confirms that we are making crystalline zinc sulfide with clear crystal lattices on the particles. Particle sizes in the range of 20 nanometers can also be seen using this HR TEM image.

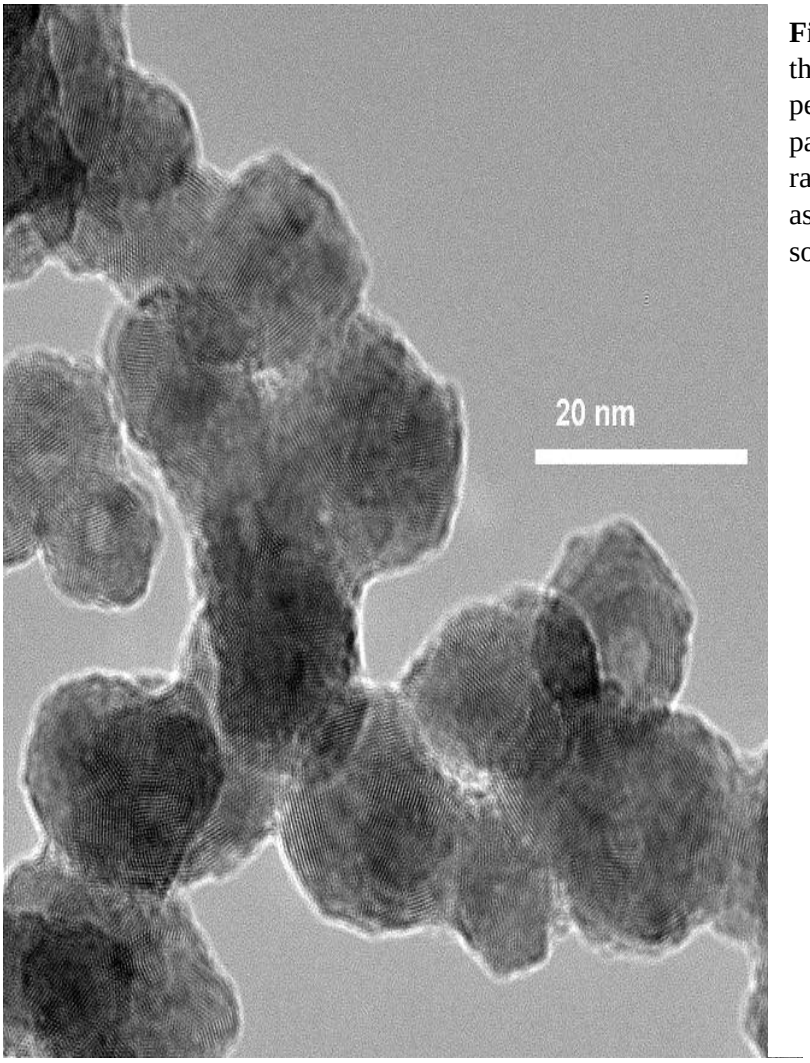

Figure 17 clearly shows the crystal lattices that persist in our ZnS particles. Particle sizes ranges from 15 to 20 nm as measured via ImageJ software.

Overall, zinc sulfide shows great promise with this technique, and has been discussed throughout the literature, ZnS stands to be a possible n-type semiconductor for use as a buffer layer for a CZTS solar cell.

4.2 Copper Sulfide

Figure 18 gives the first analysis showing that we were able to produce copper sulfide nanocrystals. Figure 18a depicts a region of similarly sized nanocrystals deposited on a standard Transmission Electron Microscope (TEM) micrograph. Figure 18b represents the dark field image associated with 18a, which is representative of a crystalline sample. Figure 18c not only shows that we have particle sizes in the range of 20nm, but it also shows clear crystal lattices. Finally, Figure 18d shows the diffraction pattern of our sample which can be indexed with ICSD to show that we were able to produce stoichiometric high chalcocite Cu_2S nanocrystals.

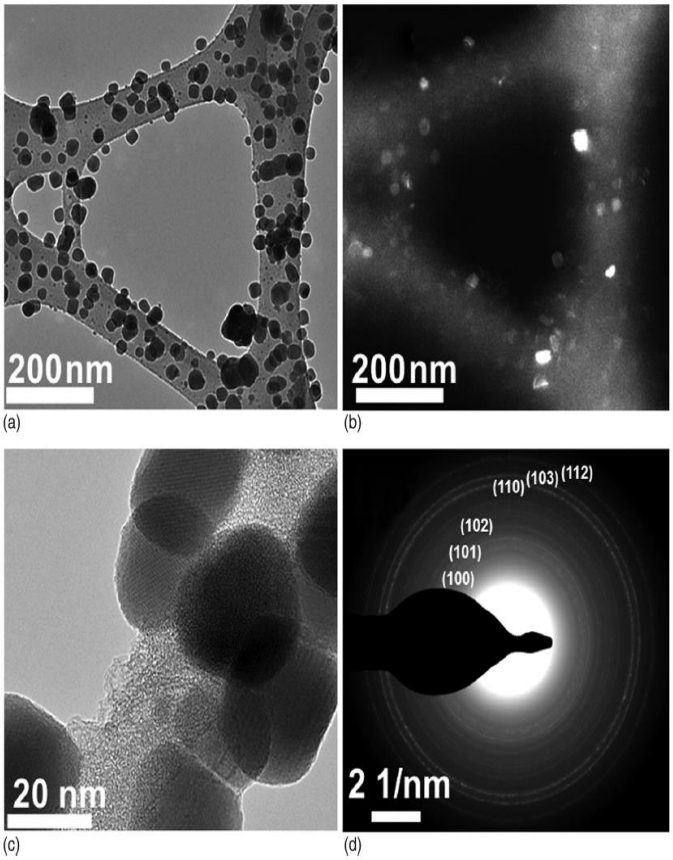

Figure 18. TEM micrographs of copper sulfide nanocrystals produced at 500°C. Dark field image, particle size, and diffraction can be observed. Particle sizes were roughly 20 nanometers in diameter. The diffraction pattern was correlated to a Cu_2S chalcocite phase, while the dark field image is representative of a typical crystalline sample of nanocrystals.

Figure from [39]

Although the nanocrystals in Figure 18 do appear to be roughly the same size in the HR TEM image, slight variation did exist. Figure 20 depicts the particle size distribution and shows that on average at a temperature of 500°C, we produce nanoparticles of 14.8 nanometers in diameter. These particle sizes were accumulated by counting multiple TEM micrographs containing hundreds of copper sulfide nanocrystals each. Particle size was measured using the image analysis software, ImageJ.

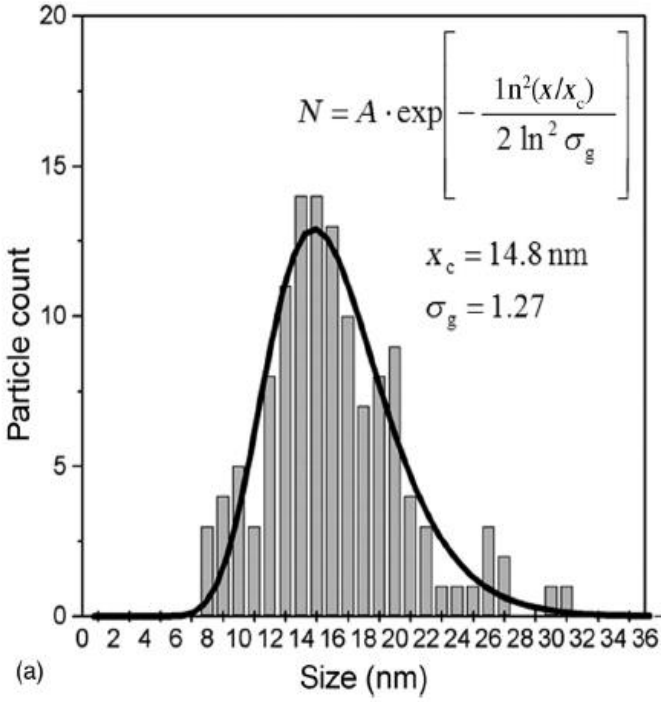

Figure 19. Particle size abundances as counted by the image analysis software ImageJ.

Figure from [39]

After analyzing these particle sizes from multiple runs, we also found that particle size was easily tunable. Merely changing the precursor concentration would change our average particle size.

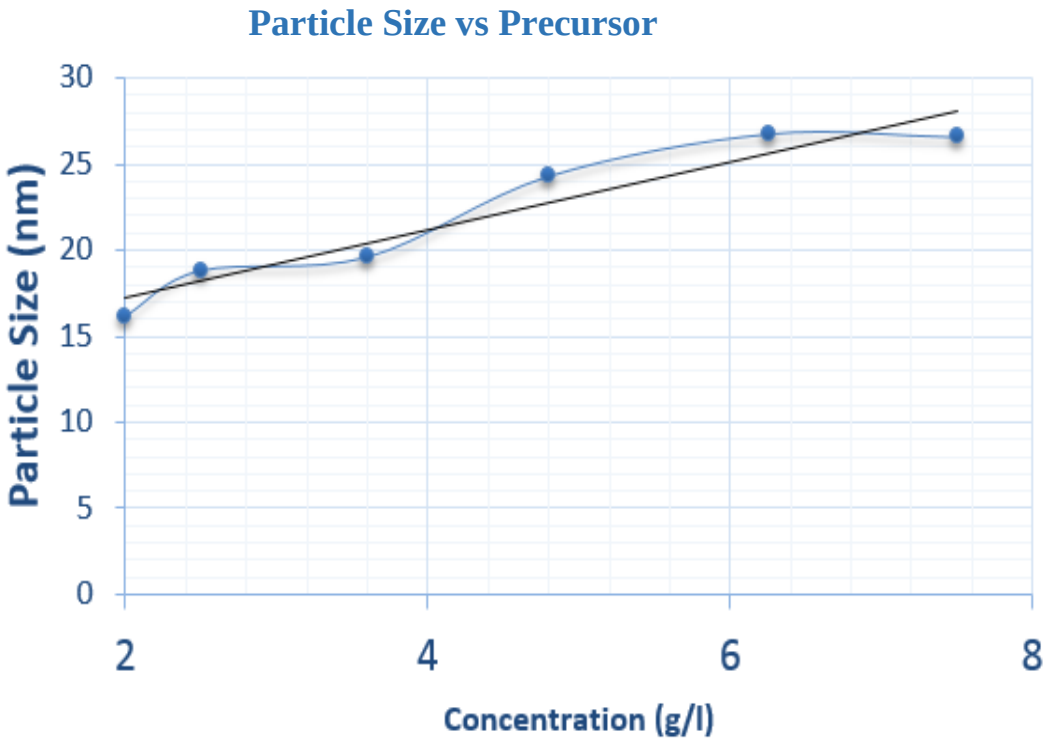

Figure 20. Precursor concentration versus particle size. We have been able to systematically correlate particle size to precursor concentration with a nearly linear relationship from concentrations of 2 mg/ml to 7 mg/ml. Particle sizes were measured using image software analysis ImageJ.

In figure 20, we have shown that particle size as compared to precursor concentration can be modeled with a linear relationship. Analyzing a wide variety of temperatures in multiple runs, we were also able to show that temperature could be directly correlated to phase state as well. Using the image software analysis ImageJ we have radially integrated the profiles and converted the data as diffraction beam intensity as a function of d-spacing and compared our samples with those of standards for digenite and chalcocite phases as seen in figure 21 [44,45]. As can be seen, we are able to tune the

phase by using the furnace temperature of the run. We see a clear transition from chalcocite phase at 500°C up to a digenite phase at 800°C. Phase tuning is very important with copper sulfide given that a wide range of phases persist, but not a wide range are extremely useful in the semiconductor field. Cu_2S is the most desirable phase to be produced, but it is very beneficial that other phases could be readily produced for other uses [44].

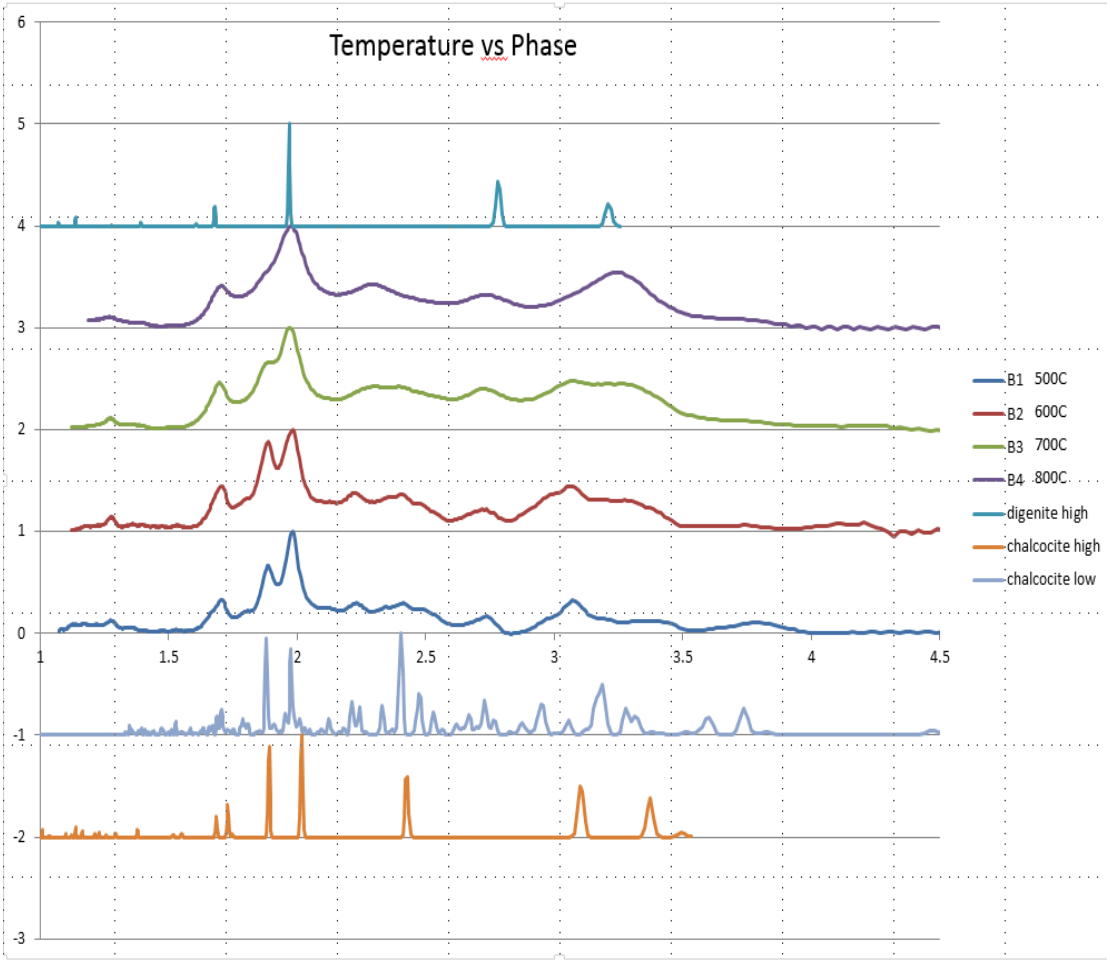

Figure 21. Selected area diffraction patterns for samples produced between 500 and 800°C are shown. Using the image software analysis ImageJ we have radially integrated the profiles and converted the data into diffraction beam intensity as a function of d-spacing. Using ICSD standards for copper sulfide in the digenite phase, $Cu_{1.8}S$ (800°C), as well as that for the low temperature chalcocite phase, Cu_2S (500°C), we have been able to show the phase tuning capability of our setup based on furnace temperature variation [44,45].

In order to verify our results obtained from analyzing diffraction ring spacing, we also used XRD to analyze a powder sample produced at a temperature of 800°C. Figure 22 represents the XRD sample we produced as compared to that from the ICSD standard for digenite. Our sample matches up very closely with a digenite phase of copper sulfide which agrees with what we saw using d-spacing from TEM diffraction patterns.

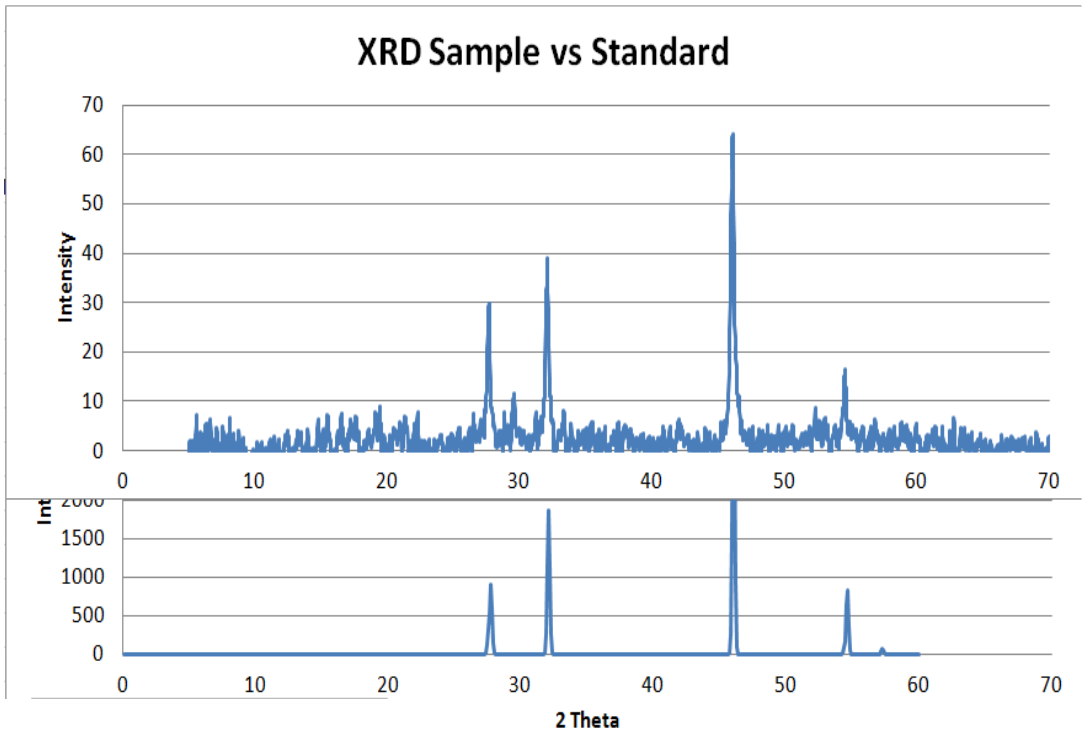

Figure 22. XRD analysis from an 800°C run on top. ICSD standard from a digenite $Cu_{1.8}S$ sample.

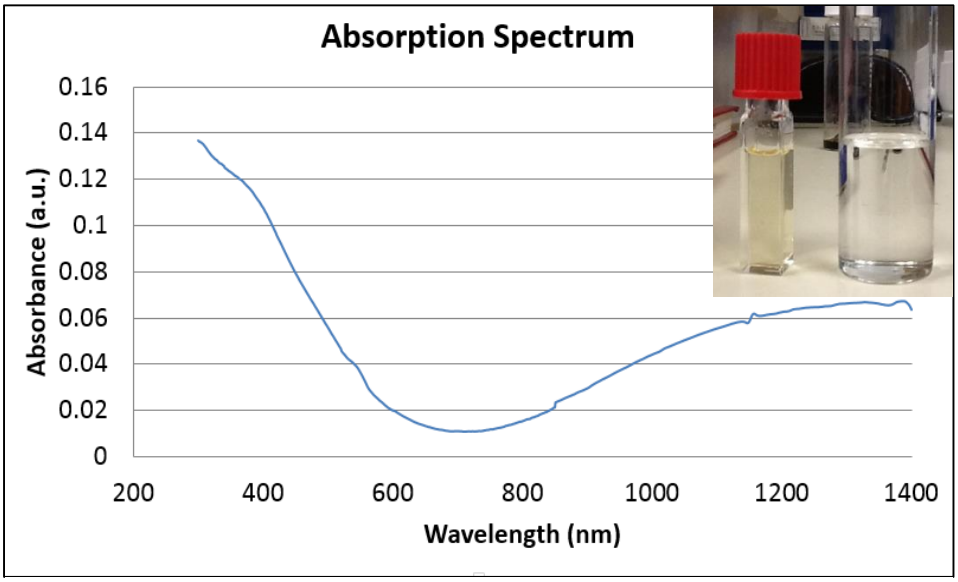

Figure 23. UV-vis absorption spectrum of 700°C sample. Absorption spectrum reflects that seen by chalcocite copper sulfide [44]. Copper sulfide sample was dissolved and diluted in chloroform as seen in Figure 23b for analysis. Figure 23b shows the copper sulfide solution in chloroform solvent on the left. Pure chloroform solvent on the right.

Figure 23 represents the absorption spectrum for a diluted solution of copper sulfide nanocrystals in chloroform. The solution was analyzed using UV-vis optical spectroscopy, and the absorption spectrum matches up well with that of a digenite phase [44]. A small shoulder can be seen right at the 450nm wavelength, which is well documented with the chalcocite copper sulfide phase [44].

$Cu(dedc)_2$ precursor produced copper sulfide nanocrystals with an efficiency of roughly 79% on average. It was also found that our setup generally produced roughly 1mg/minute with the ultrasonic nebulizer at 800°C, whereas the spray gun could produce 3 times as much in the same amount of time many factors lead to which device would be used in the future, however.

4.2.1 Device Dependence

Significant time was spent experimenting with, and attempting to create, appropriate nebulizing devices to produce copper sulfide particles. A small droplet size, a high throughput, and a reliable construction was desired. Although pressure driven aerosol devices were produced, they often proved unreliable and inconsistent.

Eventually, through trial and error, we were able to reliably produce copper sulfide nanocrystals using the three separate devices discussed earlier. Each device performed markedly differently, however. The spray nebulizer, for instance, was able to produce 3mg/min of powder at 800°C while the ultrasonic nebulizer routinely produced less than 1mg/min at the same temperature. The ultrasonic nebulizer could function at this rate repeatedly, however, and it actually never suffered mechanical difficulties during the entire extent of the research. The spray gun, on the other hand, often had problems with clogging and coagulation at the needle due to the low vacuum and concentrated solution being flown through the device. These problems often caused runs to be cut short as well. Finally, near the end of the research term, the device itself actually had to be completely replaced because it failed to function as desired. The BGI jet atomizer was very effective in producing the desired copper sulfide nanocrystals, but it also had major problems with reliability and function. The concentration of copper precursor in toluene often was near saturation point, thus, as the pressure was lowered inside the apparatus, a great deal of toluene would often evaporate out of solution. When this happened, the solution regularly would reach saturation concentration point and surpass it, leaving solid copper precursor to make nonhomogenous solution in the glass container. When this

happens, the small opening where the liquid solution is vacuum dragged through the nozzle to become an aerosol gets clogged and the device fails to function. Due to these challenges, the pressure of each of these runs had to be monitored closely. It was found that ideal pressures for using the jet atomizer were between 150-250 torr. If pressures went below 150 torr, significant clogging problems ensued. The other major challenge with the jet atomizer was that its container was made out of glass. Given the sheer number of times these experiments were performed, as well as the amount of times the devices needed to be cleaned and stored, glass posed a significant disadvantage to the atomizer. In fact, the glass was broken twice in as many months and although replacements were readily available from BGI, such a setup seemed too disadvantageous to the future of the project.

Although we did find that we could produce copper sulfide nanocrystals using the three devices described, only one device clearly met the majority of the needs of the project. The ultrasonic nebulizer was reliable and simple to use with little delicate cleaning or running parameters. It was for these reasons, too, that we chose to move forward with the ultrasonic nebulizer when we began producing CZTS nanocrystals as well.

4.3 Tin Sulfide

Tin sulfide particles were produced using the synthesis techniques discussed above. TEM analysis was the major analysis method. As can be seen in Figure 24, lattice planes are visible in the nanoscale particles produced. Figure 24b also shows these were clear crystalline material given the excellent diffraction rings. Based upon the success of the previous experiments we believe this was a crystalline material with the desired constituents. Tin sulfide was of little interest to us on its own measure, however, and thus seeing that a crystalline material with these precursors could be produced using a similar setup, we were content in moving on to attempting CZTS synthesis.

Figure 24 a.) TEM images of crystal lattice of produced particles. b.) Diffraction pattern of particles, showing clear rings which points to crystalline material. Diffraction measurement was done on sample large enough to contain hundreds of particles as seen in c.) Size perspective of nanoparticles produced on copper TEM grids.

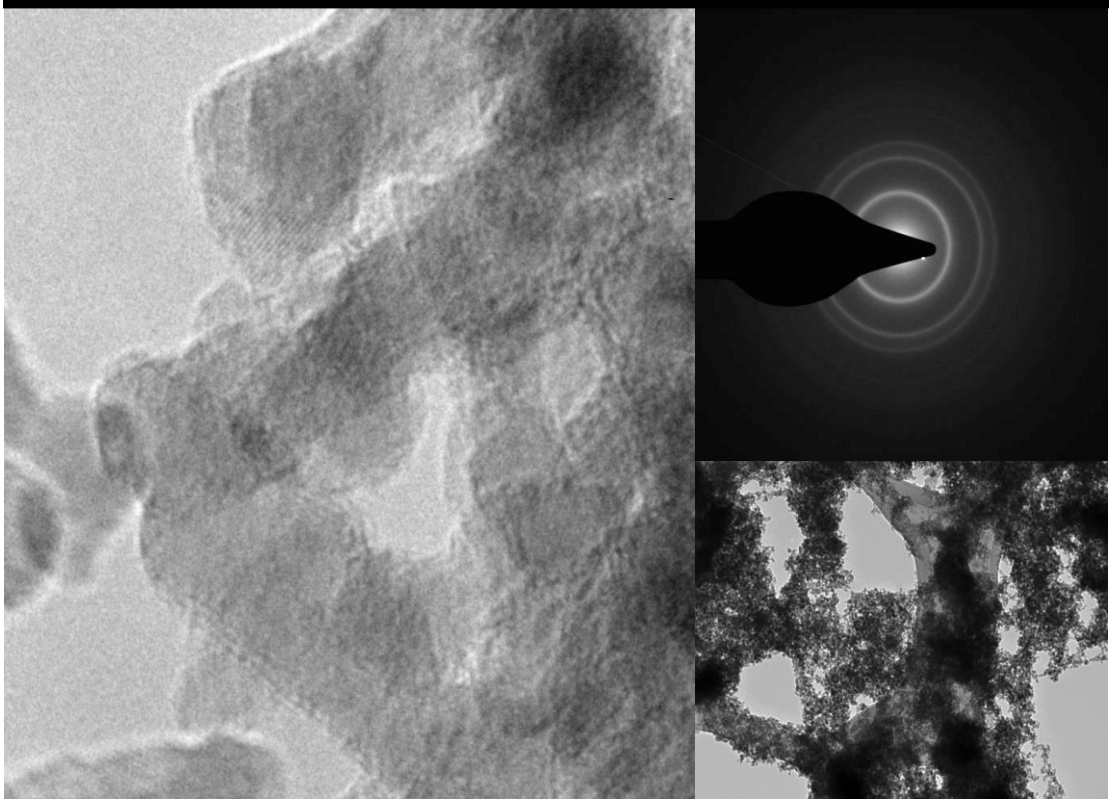

4.4 Copper Zinc Tin Sulfide Results and Discussion

4.4.1 CZTS Nanoparticle Production

As has been stated by major CZTS papers for many years, phase purity and phase identification is a major obstacle in developing CZTS in any form. As the authors in [27] have stated, the major XRD peaks are nearly identical between ZnS and CZTS. The authors in [27] as well as others attempt to identify minor peaks at 44 degrees and 37.1 degrees to be certain of the existence of CZTS. Nevertheless, these peaks are resolutely small and often subtracted with the background in many software analysis setups. Rather than rely simply on XRD analysis, many analysis techniques must be used to verify that all constituent elements are present in a specific nanoparticle sample in the correct corresponding molar ratios without extra compounds existing in the structure. Thus, to be certain we have been able to synthesize $Cu_2Zn_1Sn_1S_4$, we have used a wide variety of analysis techniques.

XRD is still a major analysis method with a large database for nearly every compound, but because of the overlap with a very possible particle of ZnS in CZTS, it cannot be relied upon solely. Nevertheless, it is important to identify the XRD peaks associated with CZTS, it just cannot be solely used to determine elemental analysis. Figure 25 shows XRD of a powder sample of CZTS produced at a temperature of 750°C. Major peaks match those associated with CZTS and ZnS as well [27].

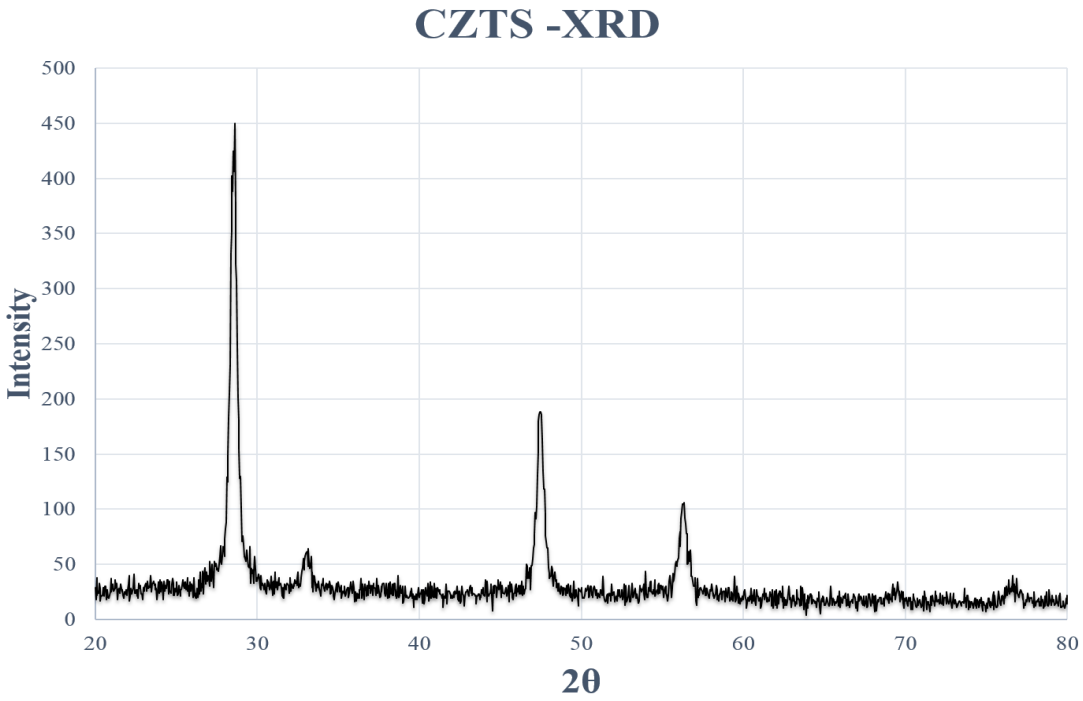

Figure 25. XRD analysis of CZTS powder sample. Major peaks have excellent agreement with stoichiometric Cu_2ZnSnS_4 as described by [27].

Raman Spectroscopy must also be used to identify peaks associated with CZTS which differs from ZnS in a fairly convincible manner. Figure 26 shows Raman spectroscopy for a powder sample produced at 750℃ and believed to be stoichiometric CZTS.

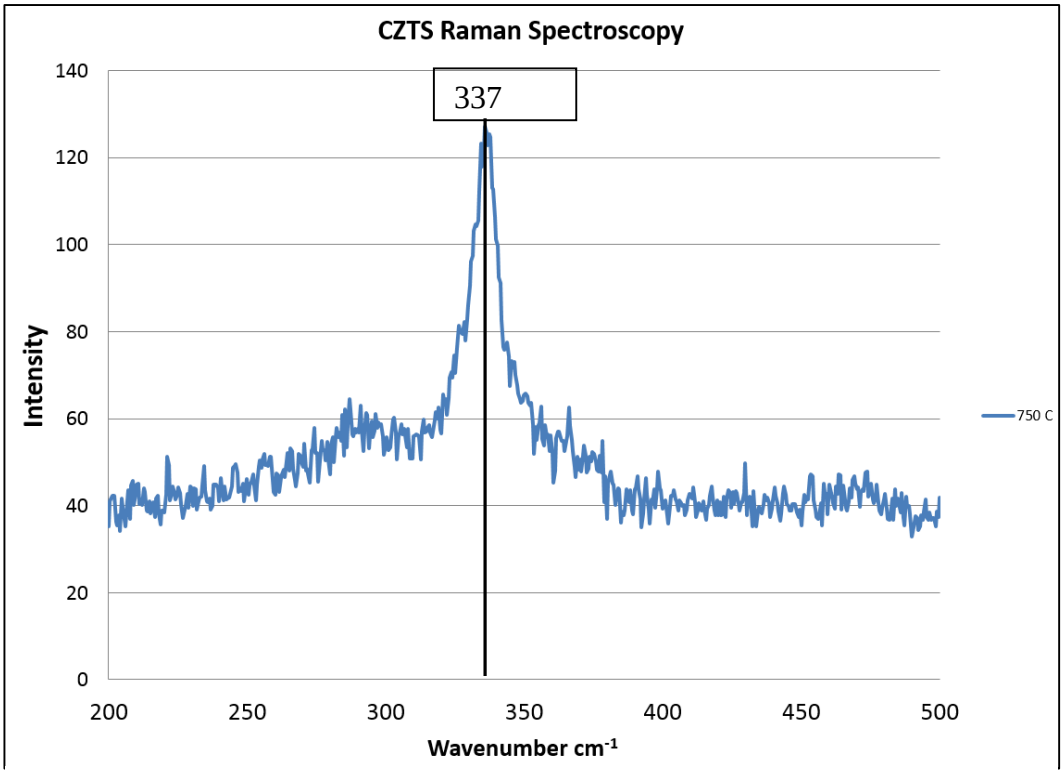

Figure 26. Raman Spectroscopy performed on a powder sample produced at 750°C. Clear peak can be seen at 337 cm^{-1} which is closely associated with that of CZTS.

Another analysis method involves energy dispersive X-ray spectroscopy (EDS). EDS allows the measurement of relative abundances of each element in a given sample. Based on these abundances, we can then standardize one of the elements to give us relative molecular abundances. Standardizing Cu with its believed ratio of two moles to one mole of zinc and tin to four moles of sulfur. In this manner, it is possible to obtain relative information about the constituents of a given sample. Figure 27 displays our most ideal sample's composition. Although it is clearly close to that of stoichiometric ratios, it is not exactly within range. The identified zinc rich composition will be discussed. Due to the manner in which EDS functions, analyzing a standard sample similar to the desired composition is highly recommended. Given the current state of CZTS technology being

solidly in the research realm, finding a realistically priced and abundant standard was not feasible for the project. To address this uncertainty, another method of elemental analysis must be used to reinforce the findings found using EDS.

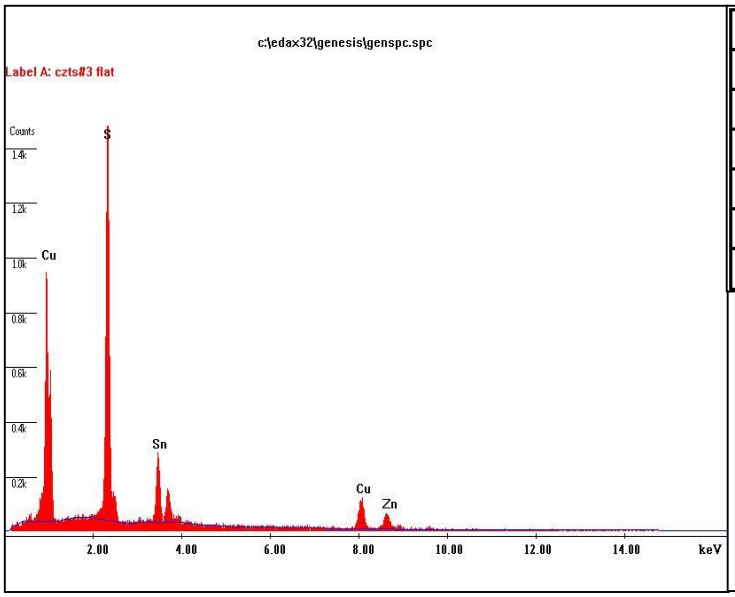

Element	Wt %	At %
S K	28.58	47.74
SnL	18.88	8.52
CuK	29.34	24.73
ZnK	23.2	19.01
Total	100	100

Figure 27 EDS results from a powder sample produced at 750°C. Based on this EDS analysis, our material had a stoichiometry of $Cu_2 Zn_{1.5} Sn_{0.7} S_{3.9}$

In order to verify our stoichiometry and further distinguish our results, XPS was done on our samples produced at 750°C. Figure 28a shows the XPS survey for our sample. Figure 28b shows a slightly different stoichiometry compared to our EDS data, but this will be further discussed in the following section. We feel that because of the nature of our powder and the fact that the XPS machine only analyses an extremely small thickness dimension, the readings from XPS cannot be completely used as confirmation versus EDS on a powder sample. Nevertheless, the stoichiometry was not far from our desired levels and thus we felt the results were still conclusive using EDS and XPS.

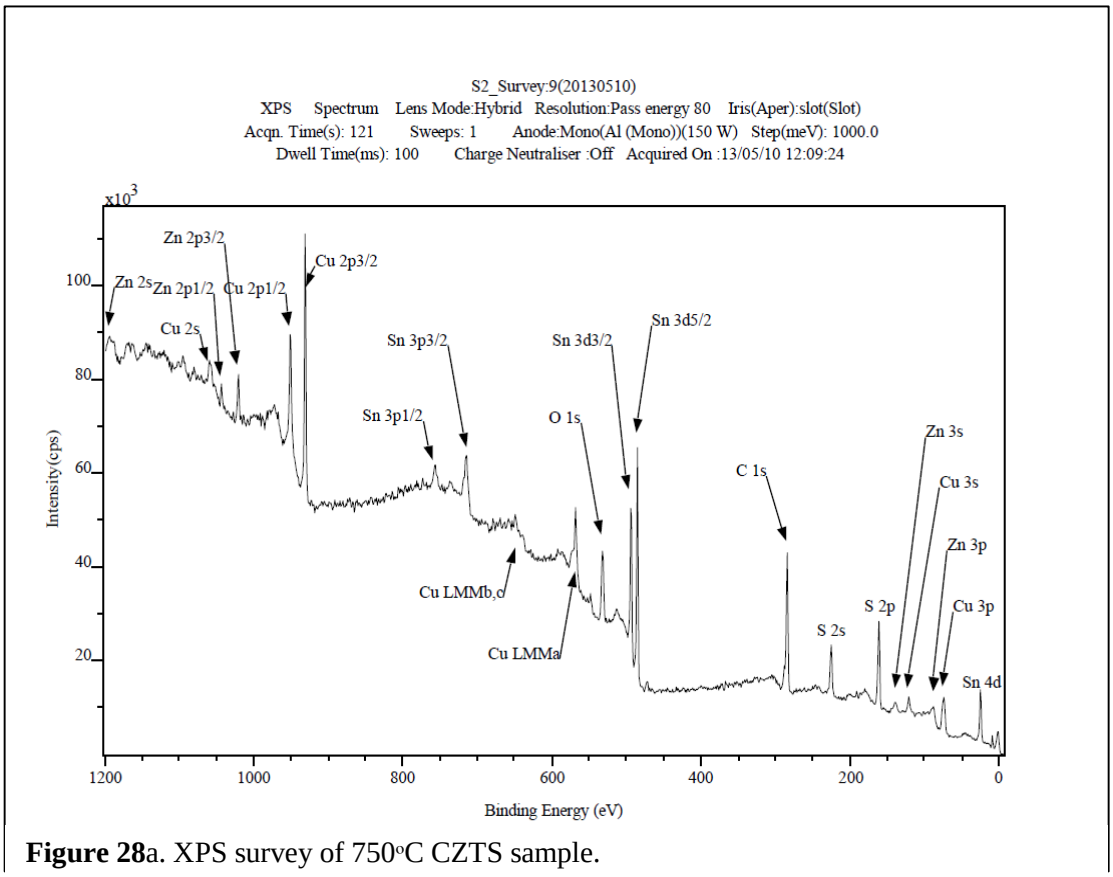

Figure 28a. XPS survey of 750°C CZTS sample.

Figure 28b. Table showing how the mole fractions are calculated. XPS shows that we had $Cu_2 Zn_{0.8} Sn_{1.1} S_{3.7}$.

	Peak Area	Sensitivity Factor	Corrected area	Atomic Percent	Mole Fraction
Zn	10292.0	5.6	1841.5	0.1	0.8
Cu	24786.0	5.3	4658.1	0.3	2.0
Sn	20389.0	7.9	2589.1	0.1	1.1
S	5780.0	0.7	8652.7	0.5	3.7

Due to the necessity of crystalline material, we also desired to see a highly magnified image of the samples to identify lattice planes. Confirmation of crystalline material was also needed. In this regard, a transmission electron microscope (TEM) was used to analyze the structure of the samples being produced. A scanning electron microscope (SEM) was also used to gain information about cross sectional analysis of the thin films as well. Figure 29 shows TEM of the CZTS nanoparticles. Dark area

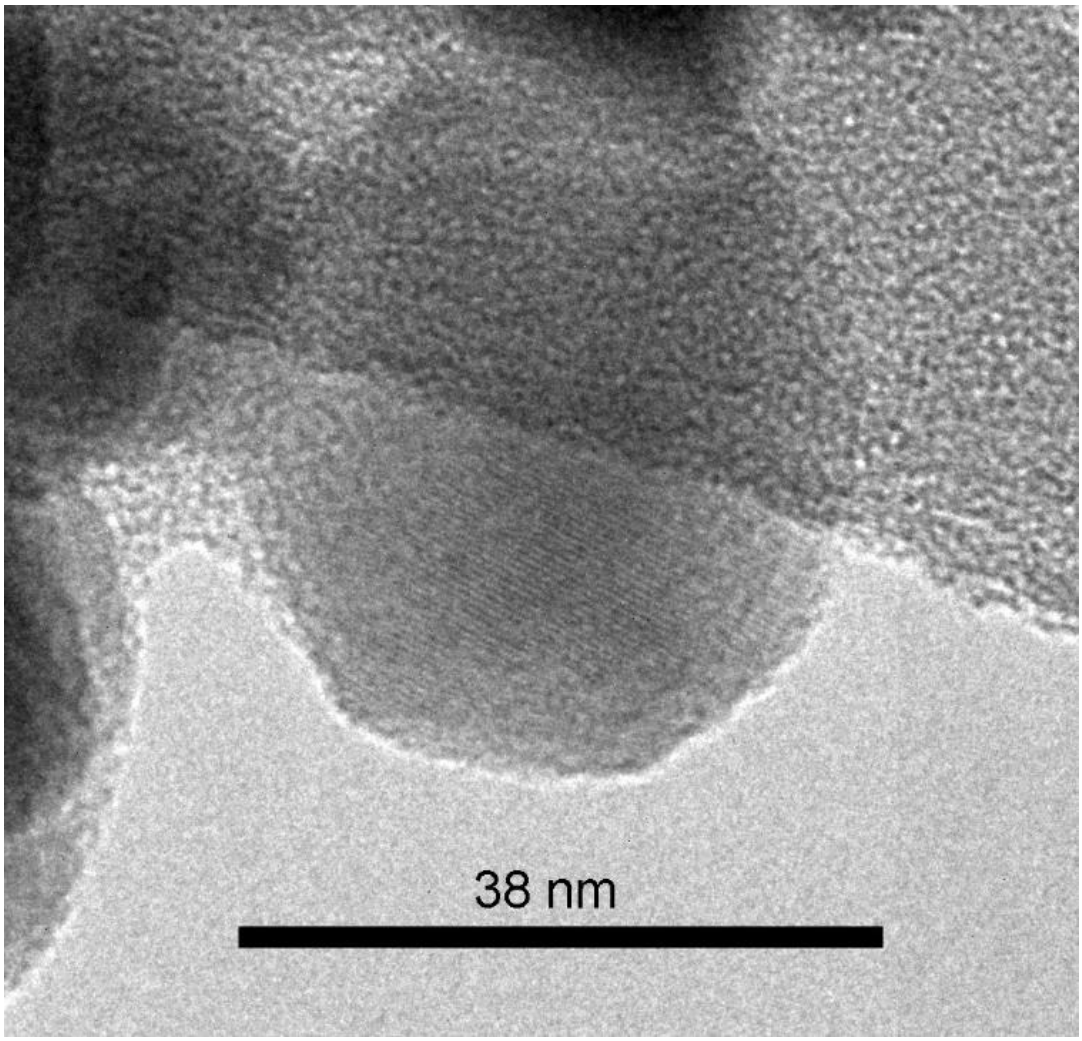

Figure 29. High Resolution TEM from a sample produced at 750°C. Clear crystal lattice fringes can be seen on this nearly 40nm particle.

diffraction pattern confirms crystalline material, and particle size is between 25-40 nanometers as calculated using ImageJ software on the TEM images.

Given that CZTS is to be used as a light absorbing layer in a solar cell, it is very important to understand its light absorption characteristics as well. Using a UV-Vis optical absorption device, we were able to gain an understanding of the absorption spectrum of our CZTS nanoparticles. The CZTS nanoparticles were dissolved into solution with chloroform as the solvent. Figure 30 shows the absorption spectrum obtained from our sample. It is evident that our material contains very similar optical properties to that of the published data from reference [46].

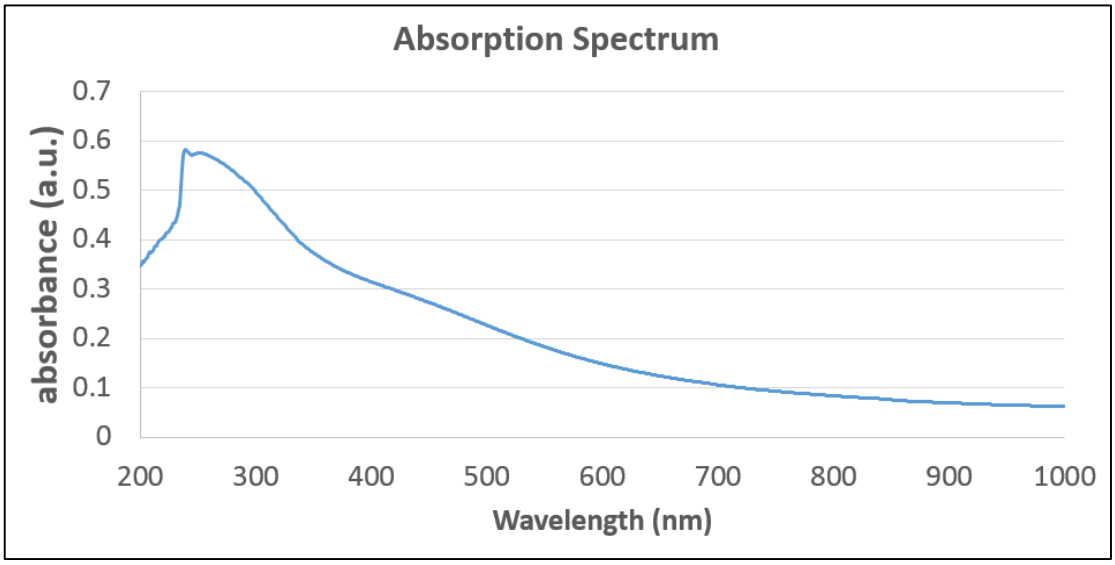

Figure 30. Absorption Spectrum on sample produced at 750°C. Spectrum matches the literature of stoichiometric CZTS [46].

4.4.1.1 Temperature Variation

Once we believed we were able to consistently produce phase pure CZTS nanoparticles, we wanted to investigate the possibility of tuning certain properties of the product. In processing this material, similar to what was accomplished with Cu_2S processing, we attempted to find the attributes which would allow the structure and properties to be tuned. As has been found by [47], CZTS phase purity is always challenging, but it is possible to isolate certain processes to tune the composition.

Figure 31 shows data from four different samples which were produced at varying temperatures. Similar to

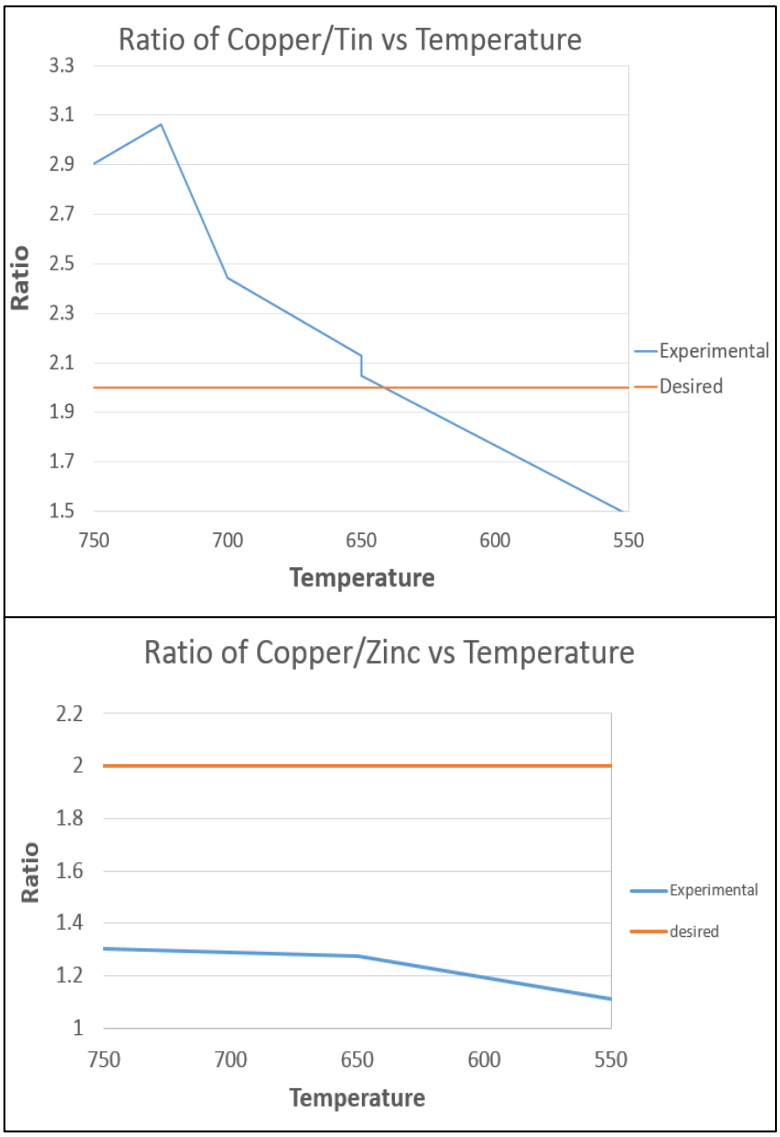

Figure 31a and b represent stoichiometric changes of Copper/Tin and Copper/Zinc with temperature. Temperature ranged from 550-750°C. Analysis was done via EDS elemental analysis. Precursor concentration and processing times were kept constant for all runs.

that shown by [48], we found that changing the temperature, while keeping all other parameters constant, had a significant effect on the composition of our samples. Specifically, as Figures 31a and 31b show, tin concentration is significantly impacted by temperature change. Specifically, lowering the temperature of the experiment from 750°C to 550°C changes the as produced samples from being tin deficient to becoming tin rich. Zinc concentration, nevertheless, is similarly affected, but at a much smaller rate simply going from zinc rich to more zinc rich. Phase purity and control is an incredibly important feature of this apparatus. Significant research exists stating the importance of the CZTS structure having an abundance of Zinc which relates to a relative deficiency of Copper [49]. The reason behind the changes, we theorize, is due to the fact that Tin has the lowest decomposition temperature of the constituent elements [50]. Thus, while the others are more stable in the heated environment, the tin decomposes out of the material at elevated temperatures quite readily.

4.4.1.2 Role of Zinc and Copper in CZTS Light Absorbing Material

A general consensus exists in the literature of the field that having an abundance of Zinc compared to the amount of copper in a given structure, actually plays a vital role in the efficiency and usability of a CZTS semi-conductor in a light absorbing device. Specifically, [49] concludes that this composition is due to an anti-site defect in the structure where a copper atom is replaced with a Zinc atom and a Sn atom is also replaced by a Zn atom. This actually makes it less common to have copper forming anti-site defects which would significantly hinder the performance of the cell. It is believed that deep defects as donors or acceptors are created when the compound is stoichiometric

or copper rich which causes significant recombination problems [source]. It also lowers the band gap significantly which is also problematic. All of these factors make the ideal Cu/(Zn+Sn)=0.8 and Zn/Sn=1.2 [49].

Figure 32 shows a stoichiometric CZTS structure. 32a) shows a kesterite structure which is widely accepted as the ideal setup b) represents a stannite structure and c) represents a much less common PMCA structure. The Zn_{Cu} antisite defect would replace the white copper atoms with the purple zinc atoms. It is believed that the Cu also leaves many vacancies as well as antisite defects. Nevertheless, the literature explains that this allows easier hole transport and greater efficiencies overall [27].

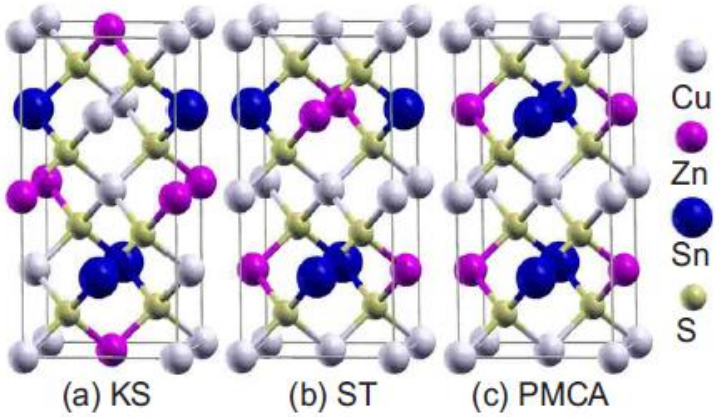

Figure 32. Common structures of CZTS. a) Kesterite is believed to be the most common and agreed upon best structure for use in light absorbing materials.

Figure from [27]

4.4.1.3 Aerosol Variation and Powder Production

Figure 33 displays the device we have solely used to develop CZTS nanoparticles. Through steadfast experiments attempting to produce copper sulfide nanoparticles we had determined that the ultrasonic nebulizer is most suitable to reproducibly synthesis CZTS. Due to the energy dispersion of the liquid inside, we found that the less volume of precursor inside the nebulizer, the faster powder production occurred. From experimentation it appeared that roughly 15 ml of precursor inside the nebulizing chamber at any given time would produce the fastest powder production of roughly 1.5 mg per min. To allow a larger amount of powder to be produced in a smaller amount of time, as shown in figure 14, a system to keep the liquid level at optimal operating levels was integrated. This allowed liquid allotments of precursor to be inserted during runs to allow for greater production as well.

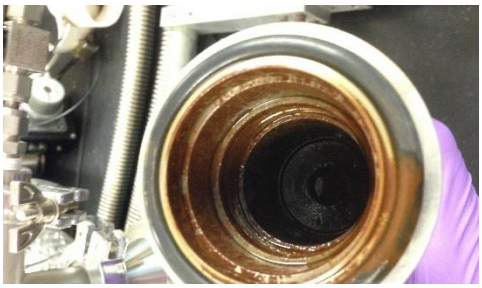

Figure 33 Inside of empty ultrasonic nebulizer

4.4.2 Thin Film Results and Discussion

Thin films were grown upon a range of substrates. SEM images best show the cross section of the CZTS crystals grown on substrates of molybdenum coated glass and oxidized silicon wafers. Figure 34 shows the slight variation of films grown on different substrates.

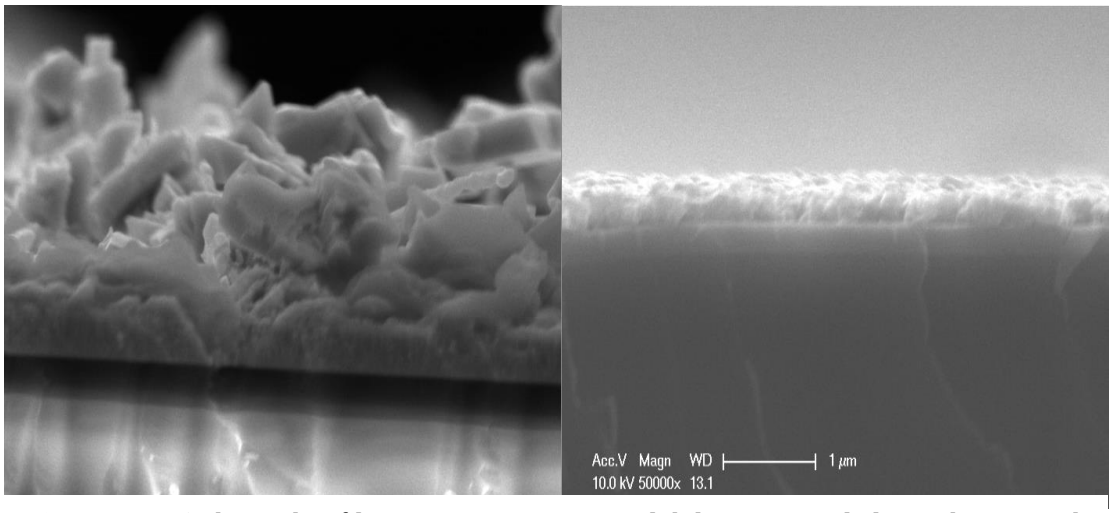

Figure 34. A.) shows thin film CZTS grown on a molybdenum coated glass substrate. 34b shows a CZTS thin film grown on an oxidized silicon wafer. Both samples were produced at 450°C and run for 20 minutes. Thin film A is nearly 500 nm in thickness while film B is only 250 nm in thickness.

Figure 35 shows XRD analysis from a sample grown at 450°C on an oxidized silicon wafer for 25 minutes. A standard from ICSD database is graphed with our sample to show its agreement. Using the FWHM value, wavelength of the incident X-ray source, and peak position, the grain size can be calculated using the Scherrer equation. We calculated that the grain size of this sample was 43 nanometers.

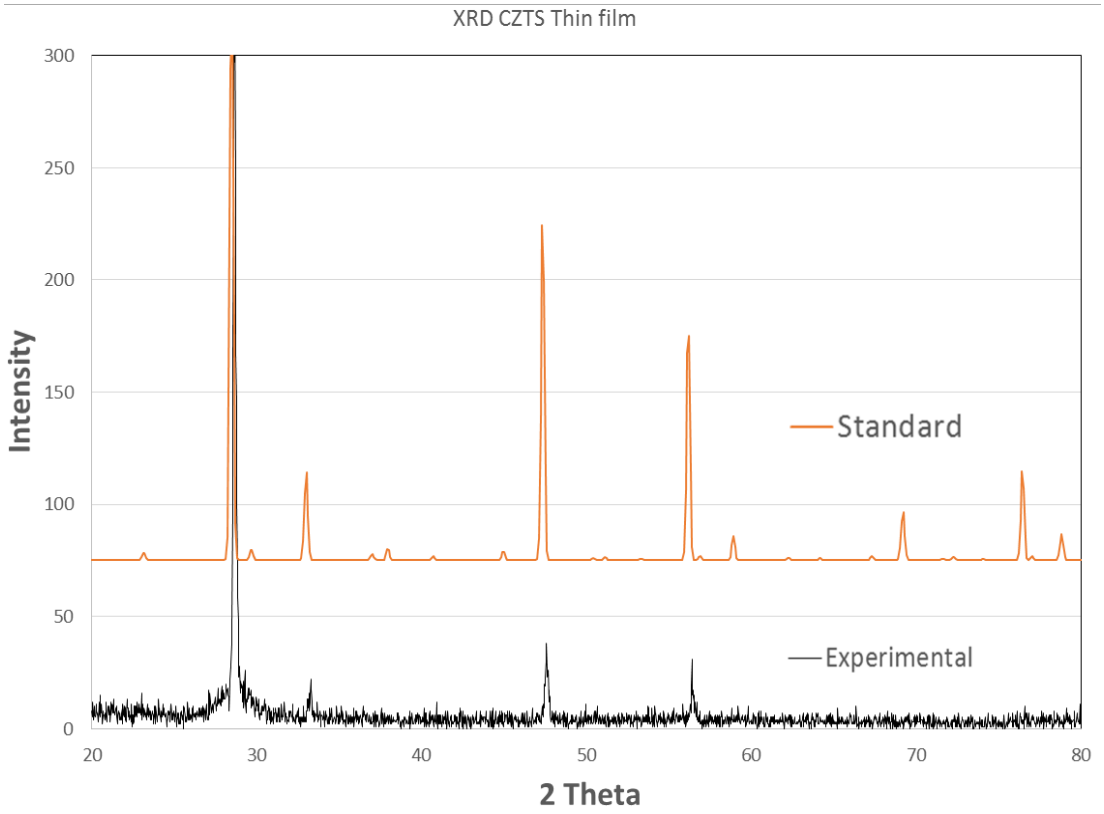

Figure 35. XRD analysis of film grown at 450°C as compared to an ICSD standard for kesterite CZTS. Grain size of sample was determined to be 43 nanometers as calculated using the Scherrer equation.

Figure 36 displays the relation between sputtering time and composition from XPS analysis. Sputtering removes roughly 2nm in depth per minute, thus the total depth should be around 60nm into the material for these results. We hypothesize that the

stoichiometric difference of the surface and the bulk could be from the effect of processing. The bulk material is in the heating chamber slightly longer. Similar to annealing, it may be that the surface particles have not grown into similar crystalline structures like the bulk due to this reduced heating time on the substrate. Much greater analysis is necessary to confirm this theory, however, and it would be an interesting study for the future of the project. Overall, this data shows that the bulk material when analyzed

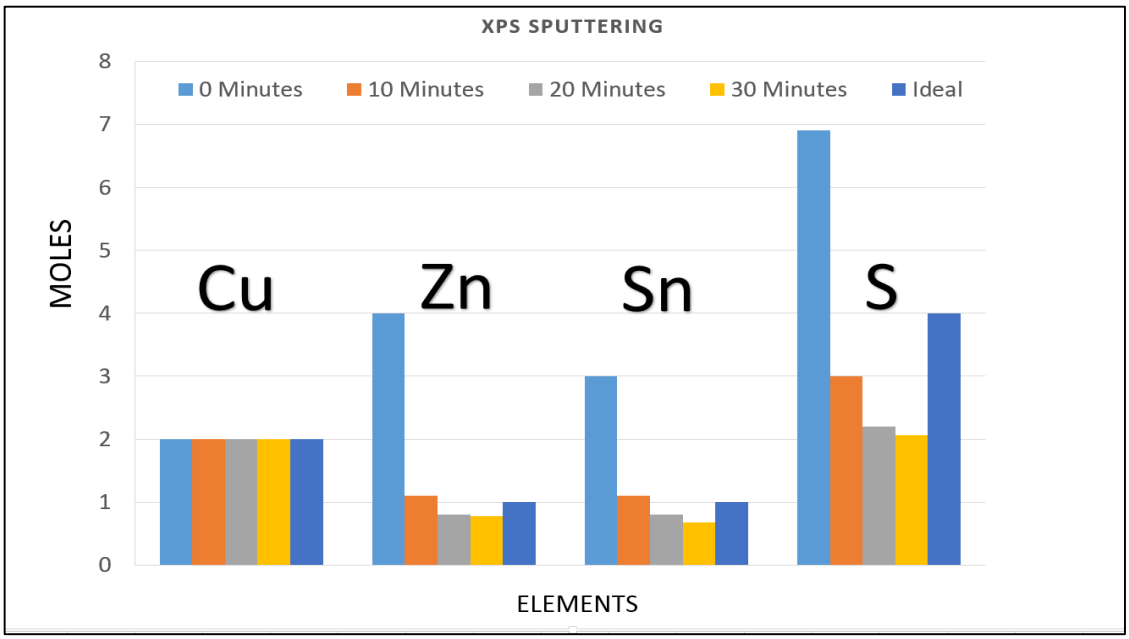

Figure 36. XPS ion sputtering sample. Elemental relative concentrations versus sputtering time in minutes. Although sputtering shows that our material characterization done using EDS can be trusted, it still shows that our samples are sulfur deficient. This is common, however, and will be discussed. Copper atomic ratios were set as the standard so the other atomic ratios could be calculated.

with XPS shows excellent agreement with the data found using EDS as shown in Figure 37. Composition of the material as analyzed by EDS shows $Cu_2Zn_{0.9}Sn_{0.7}S_{2.6}$ whereas with XPS in the bulk shows $Cu_2Zn_{0.8}Sn_{0.7}S_{2.1}$ which shows quite good agreement. It is from this analysis that we conclude that the EDS results obtained here and in previous analysis can be considered to be reliable measurements for our samples.

Figure 37 shows the XPS surveys and EDS data from our sample taken before sputtering and after 30 minutes of sputtering. The copper peak which resides between 970-920ev grows significantly in relative intensity height as compared to those of the zinc and tin peaks which reside from 1070-1010ev and 505-475ev respectively. Overall, though, the scan helps reaffirm our previous EDS results.

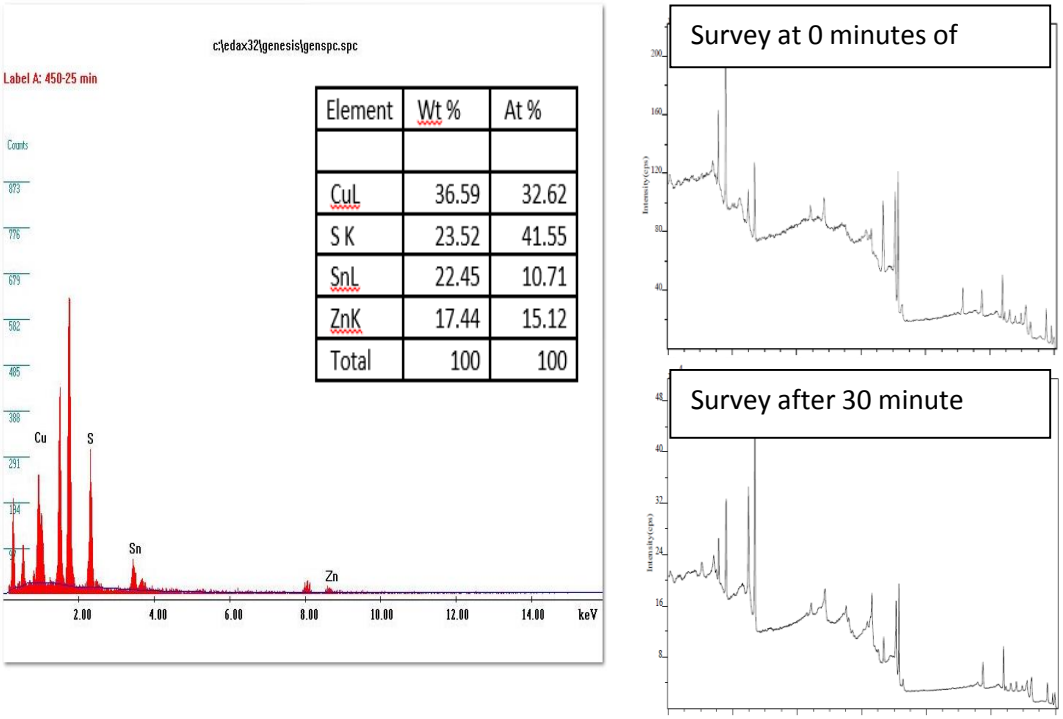

Figure 37. Figure 37a represents the EDS scan of the sample which was run at 450°C and grown on an oxidated silicon wafer for 25 minutes. The sample was then analyzed separately by EDS and XPS to compare machine accuracy and agreement. The table displays the relative atomic percent of each element. Figure 37b, XPS scan before sputtering. Figure 37c, XPS scan after argon 4kv sputtering.

Raman Spectroscopy in Figure 38 shows agreement with the accepted peaks of CZTS thin films with a major peak at 337 cm^{-1}. Minor peaks at 288 cm^{-1} and 371 cm^{-1} can be established as well [36]. One of the peaks that is not a desirable peak, is that at 221. This is not a major peak typically associated with CZTS, but it has been stated as a

minor peak from a ZnS raman spectra [36]. Nevertheless, the main Raman peaks for ZnS are 351 cm^{-1} and 273 cm^{-1} [51]. These peaks cannot be easily established due to the width of the major peak of CZTS and the flat peak at 288 cm^{-1}, but we do not see a peak with intensity similar to that at 337cm^{-1}, which would seem that we do not have a ZnS phase impurity upon first inspection. Greater levels of analysis will be needed to be certain, however.

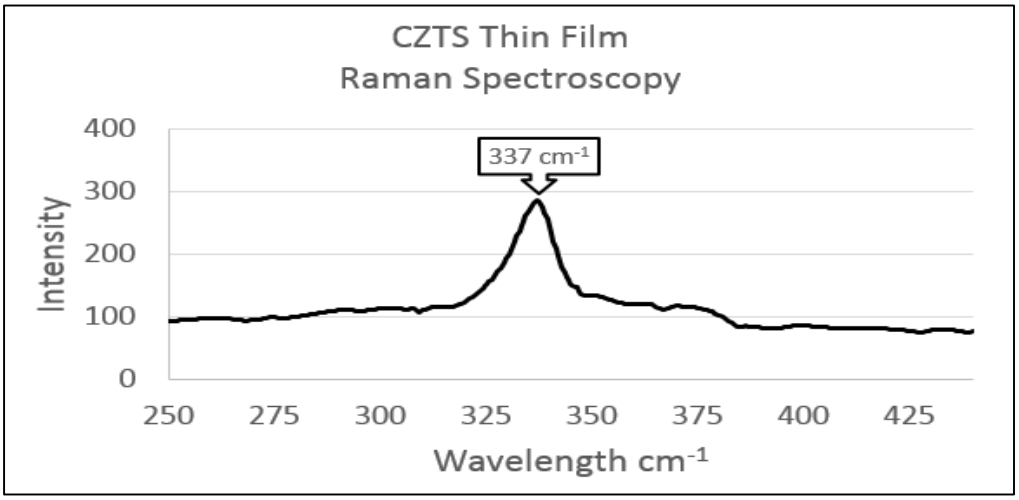

Figure 38. Raman spectroscopy of our sample produced at 450℃ on a Swiss glass substrate using a 532nm wavelength Raman laser.

Figure 39 represents the absorbance spectrum of CZTS produced on a glass substrate and analyzed using a UV-vis spectroscopy device. These absorption spectrums shows good absorbance in the desired range with fallout after 1000nm as is expected of CZTS thin films.

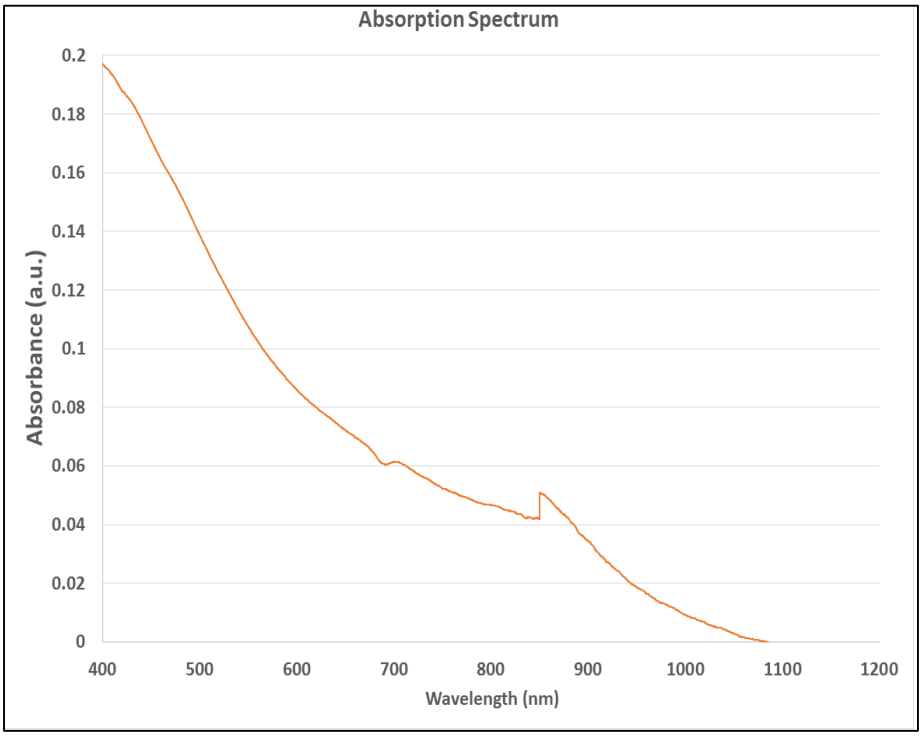

Figure 39. UV-vis absorption spectrum of a sample grown at 450°C on Swiss glass for 25 minutes. The incongruence near 900nm is due to the device and not related to the sample properties.

Using EDS analysis, the majority of our samples grown at 450°C were fundamentally, significantly sulfur deficient, which is almost unanimously seen in vacuum based synthesis methods of thin film growth in this field [37,42,33-35]. To address this, a further step involving annealing commonly takes place. Annealing typically takes place in a sulfur environment which is either developed by using H_2+S gas, or an inert environment where solid sulfur pellets are placed in a holding device to

be vaporized to create a sulfurous environment [33-35,37,42]. The system is usually either vacuumed or sealed from oxygen and other contaminants at atmospheric pressure. Typical annealing temperatures occur at 500°C which is much higher than the temperature needed to let the sulfur pellets vaporize but this temperature allows grain growth in the structure and has been shown to be near ideal [42]. Trials have begun in our setup to see if we can have similar success as reported in numerous pieces of literature [33-35,37,42].

Figure 40 shows a cross section of a thin film grown at 450°C for 25 minutes on a molybdenum coated Swiss glass substrate. Grain size was measured to be 43 nm as reported previously. Nevertheless, the annealing step is still necessary to increase grain size and incur the needed sulfur the structure currently lacks.

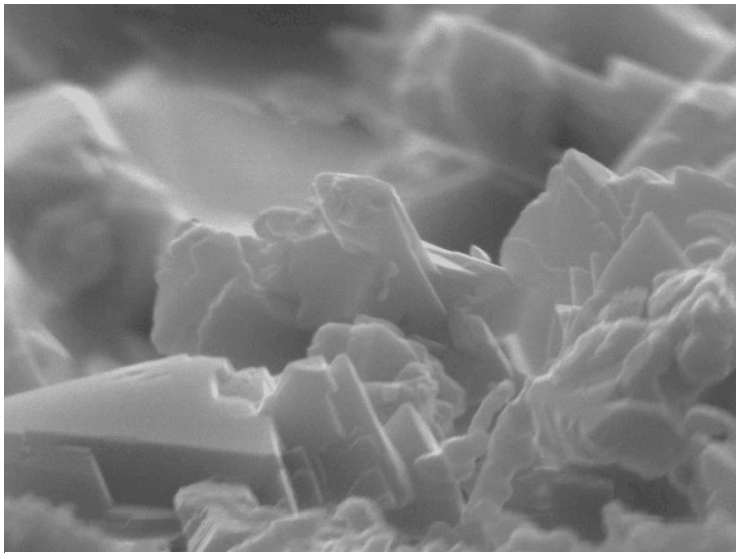

Figure 40, cross section of 450°C thin film grown for 25 minutes on a Mo-coated, Swiss glass substrate and cleaved to see cross section.

4.4.3 Preliminary Annealing and Concentration Variation Experiments

Figure 41 shows preliminary results of our annealing attempts. Substrates were heated in a sulfur environment where 400mg of sulfur pellets were contained 6cm from CZTS thin film on Swiss glass substrate. Initial results show that this setup may be one in which we are able to grow stoichiometric CZTS thin films. Nevertheless, a greater amount of experimentation and analysis is necessary to verify grain growth and reproducibility of this setup.

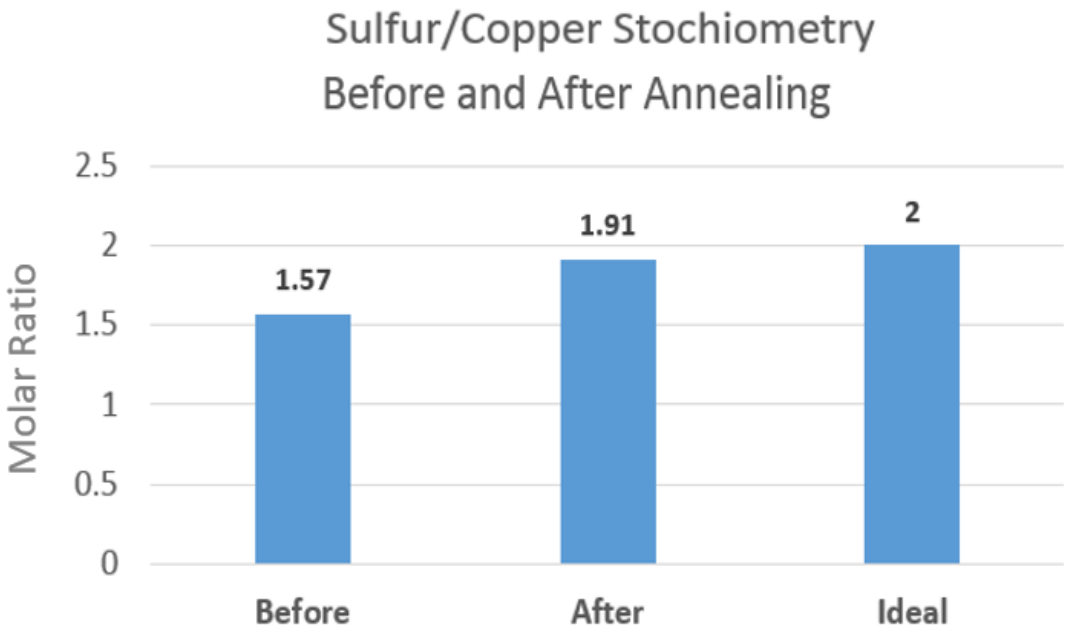

Figure 41. Analysis via EDS shows that initial annealing attempts have positive results. Substrates were heated in a sulfurous environment for 20 minutes at 500°C.

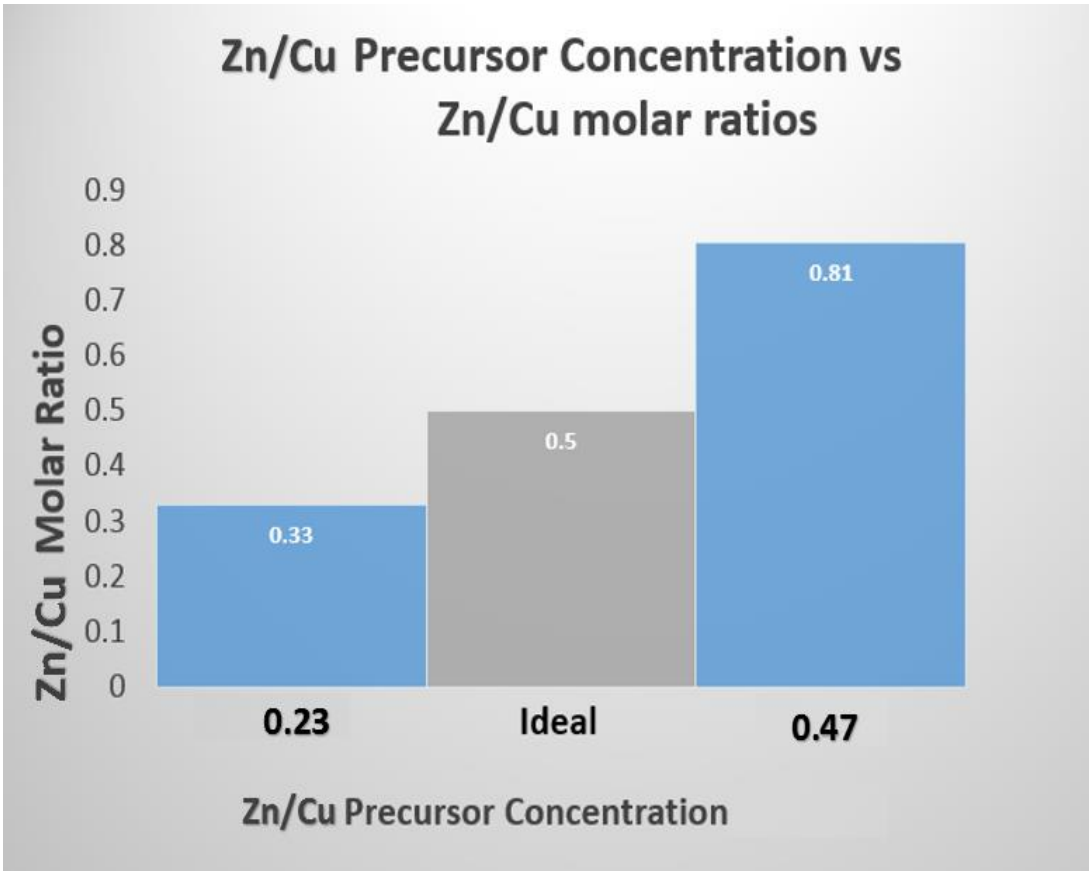

Figure 42. EDS data after initial experiment varying Zinc precursor concentration. Films were grown on Swiss glass substrates at 450°C. Copper and Tin precursor concentrations were kept constant for these films. If we extrapolate this data, we would estimate that a precursor concentration ratio of .35mg of zinc precursor to every 1mg of copper precursor would give ideal stoichiometry in a CZTS thin film.

Figure 42 displays our initial results from varying precursor concentration to change stoichiometry. Only zinc concentrations were varied for these results, and it shows that we nearly have a linear relation between zinc precursor concentration and film composition molar ratio. More analysis will be further studied, but it does appear that tuning of precursor concentration has a direct effect on final film stoichiometry. Nevertheless, future works will need to be done to verify these initial results and find the ideal precursor concentrations for the desired films to be grown.

5. CONCLUSION AND RECOMMENDATIONS

In developing this approach, many considerations were made to be able to produce ink dispersions of Copper Zinc Tin Sulfide nanoparticles which could be used in roll-to-roll fabrication of CZTS solar cells. An ink dispersion could simply involve the dissolution of the CZTS nanoparticle powder into a solvent such as chloroform or toluene, where it could then be applied in multiple swaths to produce a given thickness of material onto a substrate for use as a light absorbing layer of photovoltaic device. [52,53] have used this ink dispersion method to produce CZTS layers in their experiment as well. Nevertheless, given the constraints of a master's program, and the many hurdles encountered related to the difficulties of choosing a specific synthesis technique as well as the usual hardware failures and setbacks, this ink was not able to be produced. Of course, the future of the project will need to investigate the feasibility of this powder as an ink, but it will also need to construct an actual solar cell. Given that this project was able to produce powder and thin films, an excellent and direct comparison of efficiencies of a device using the same synthesis techniques but different growth mechanisms (thin film vs bulk ink dispersion) will make for an excellent analysis and understanding of the material developed as well.

Before the cell can be produced using the thin film or nanocrystal developed, a further tuning of the annealing process is necessary. Once a solar cell is developed, however, efficiency calculations will be incredibly interesting, and I look forward to hearing about this in the future. Given that a buffer layer of ZnS could be used, it would be possible to produce a truly nontoxic, earth abundant, affordable solar cell.

In conclusion, it would appear that both a thin film and a bulk powder material of CZTS were produced using this novel synthesis technique. Using TEM, XRD, XPS, EDS, and SEM we feel that we have sufficiently characterized our material to be of the correct stoichiometry but still ideally Zinc rich. Although further investigation and solar cell construction are desirable to fully measure the effectiveness and overall usefulness of the as produced material, it seems promising. The technology and material potential look to have the possibility to truly lead the industry and the global energy market much further into the realm of realistic levels of renewable energy production and consumption to allow us to continue to enjoy our current planet.

References

[1] Department of Energy. Annual Trends. July 2013.
<< http://www.eia.gov/renewable/annual/trends/ >>

[2] "Cancun Agreements." United Nations Framework Convention on Climate Change. Web. 29 Nov. 2010. <<http://www.unfccc.int>>.

[3] William R. L. Anderegg, James W. Prall, Jacob Harold, and Stephen H. Schneider Expert credibility in climate change. PNAS 2010 107: 12107-12109.

[4] U.S. Energy Information Administration, Annual Energy Review, August 19, 2010

[5] Peter Menzel Photography. July 2013.
<<http://menzelphoto.photoshelter.com/image/I0000luMSr5mNeTw>>

[6] Department of Energy, Energy Efficiency and Renewable Energy Clearinghouse, "Concentrating Solar Power: Energy from Mirrors," March 2001.
<<http://www.nrel.gov/docs/fy01osti/28751.pdf>>

[7] D. M. Chapin, C. S. Fuller, and G. L. Pearson (May 1954). "A New Silicon p-n Junction Photocell for Converting Solar Radiation into Electrical Power". Journal of Applied Physics 25 (5): 676–677

[8] Klein, J. (2009) Comparitive Costs of California Central Station Electricity Generation, Tech.rep., California Energy Commission.

[9] Introduction to Photovoltaic Devices. PVeducation.com. July 2013.
<<http://www.pveducation.org/pvcdrom/introduction/introduction>>

[10] T. Tiedje, E. Yablonovitch, G. D. Cody, and B. G. Brooks, "Limiting Efficiency of Silicon Solar Cells," IEEE Trans. Electron. Dev. 31(5), 711–716 (1984)

[11] A. Goetzberger and C. Hebling. Photovoltaic materials, past, present, future. Solar Energy Materials and Solar Cells, Volume 62, Issues 1‑2, 15 April 2000, Pages 1‑19

[12] Jefferson Labs. The Element Silicon. July 2013
<< http://education.jlab.org/itselemental/ele014.html>>

[13] Wikipedia. List of CIGS companies. July 2013
<< http://education.jlab.org/itselemental/ele014.html>>

[14] National Renewable Energy Laboratory. CIGS PV Technology: Challenges, Opportunities, and Potential. July 2013. <<http://microlab.berkeley.edu/text/seminars/slides/Noufi.pdf>>

[15] W. Shockley and H. J. Queisser, "Detailed Balance Limit of Efficiency of p-n Junction Solar Cells." Journal of Appied. Physics, vol. 32, 510-519, Mar. 1961.

[16] Fthenakis, V. M. 2003. Overview of Potential Hazards. Chapter VII-2, Practical Handbook of Photovoltaics: Fundamentals and Applications. Elsevier, ISBN 1-856-17390-9.

[17] H. Wang. "Progress in Thin Film Solar Cells Based on Cu2ZnSnS4," International Journal of Photoenergy, 2011

[18] H. Katagiri, N. Sasaguchi, S. Hando, et al. "Preparation and evaluation of Cu2ZnSnS4 thin films by sulfurization of E-B evaporated precursors" Solar Energy Materials and Solar Cells 49 (1997) 407-414

[19] T. Todorov, J. Tang, S. Bag, O. Gunawan, et al, Advanced Energy Materials, 3, (2013), 34-36.

[20] S. Abermann. Solar Energy 94 (2013) 37-70

[21] Delbos, S., 2012. Kesterite thin films for photovoltaics: a review. EPJ Photovolt. 3, 35004

[22] S. Y. Chen, X. G. Gong, A. Walsh, and S. H. Wei, Appl. Phys. Lett. 96, 021902 (2010).

[23] Q. Guo, G. M. Ford, W-C. Yang, et. al. J. AM. CHEM. SOC. 2010, 132, 17384–17386

[24] D. Barkhouse, O. Gunawan, T. Gokmen, et. al. Prog. Photovolt: Res. Appl. 2012; 20:6–11

[25]W-C. Hsu, B. Bob, W. Yang, et al. Energy Environ. Sci., 2012,5, 8564-8571

[26] D. A. R. Barkhouse, O. Gunawan, T. Gokmen, et al. Prog. Photovolt: Res. Appl. 2012; 20:6–11

[27] A. J Cheng, M. Manno, A. Khare, et al. J. Vac. Sci. Technol. A 29 (5) Sep/Oct 2011.

[28] H. Yang, L. A. Jauregui, G. Zhang, et al. Nano Lett. 2012, 12, 540−5

[29] H. Katagiri, K. Jimbo, K Moriya, et al. “SOLAR CELL WITHOUT ENVIRONMENTAL POLLUTION BY USING CZTS THIN FILM” 3rd World Conference on Photovoltiaic Energy Conversion May 11-18, 2003. Osaka, Japan.

[30] H. Katagiri, K. Jimbo, W. S. Maw et al. / Thin Solid Films 517 (2009) 2455–2460

[31] Wikipedia. Electron beam physical vapor deposition. July 2013. <<http://en.wikipedia.org/wiki/Electron_beam_physical_vapor_deposition>>

[32] Wikipedia. Sputtering. July 2013 <<http://en.wikipedia.org/wiki/File:Sputtering.gif>>

[33] A. Khalkar, K.-S. Lim, S-M. Yu, et al. “Effect of Growth Parameters and Annealing Atmosphere on the Properties of Cu2ZnSnS4 Thin Films Deposited by Cosputtering,” International Journal of Photoenergy, vol. 2013, Article ID 690165, 7 pages, 2013.

[34] S. W. Shin, S.M. Pawar, C. H. Park, et al. Solar Energy Materials & Solar Cells 95 (2011) 3202–3206

[35] A. I. Inamdar, K-Y. Jeon, H. S. Woo, et al. ECS Transactions, 41 (4) 167-175 (2011)

[36] C. Steinhagen, M. G. Panthani, V. Akhavan,, et al. J. AM. CHEM. SOC. 2009, 131, 12554–12555

[37] W. Daranfed, M.S. Aida, N. AttafJournal, et al. Journal of Alloys and Compounds 542 (2012) 22–27

[38] A. Khare, A.W. Wills, L.M. Ammerman, D.J. Norris, and E.S. Aydil: Size control and quantum confinement in Cu2ZnSnS4 nanocrystals. Chem. Commun. 47, 11721 (2011).

[39] P. Davis and L. Mangolini. MRS Communications / Volume 3 / Issue 01 / 2013, pp 57-60

[40] C. Girotto, B.P. Rand, J. Genoe, and P. Heremans: Exploring spray coating as a deposition technique for the fabrication of solution-processed solar cells. Sol. Energy Mater. Sol. Cells 93, 454–458 (2009).

[41] S. Liu, H.W. Zhang, and M.T. Swihart: Spray pyrolysis synthesis of ZnS nanoparticles from a single-source precursor. Nanotechnology 20, 235603 (2009).

[42] N.M. Shinde, R.J. Deokate, C.D. Lokhande. Journal of Analytical and Applied Pyrolysis 100 (2013) 12‑16.

[43] P.M. Madhusudanan, K.K.M. Yusuff, and C.G.R. Nair: Thermal-decomposition kinetics of diethyldithiocarbamate complexes of copper(II) andnickel(II). J. Therm. Anal. 8, 31–43 (1975).

[44] U. GAUTAM and B. MUKHERJEE. Bull. Mater. Sci., Vol. 29, No. 1, February 2006, pp. 1–5.

[45] M. Krunks, E. Mellikov and 0. Bijakina. Physica Scripta. Vol. T69, 189-192, 1997

[46] S. C. Riha, B. A. Parkinson, A. L. Prieto. J. AM. CHEM. SOC. 2009, 131, 12054–12055

[47] H. Yoo, J.H. Kim, L. Zhang. Current Applied Physics 12 (2012) 1052-1057
[48] S. C. Riha, B. A. Parkinson, and A. L. Prieto. J. Am. Chem. Soc., 2011, 133 (39), pp 15272–15275

[49] S. Chen,L-W. Wang, A. Walsh. APPLIED PHYSICS LETTERS 101, 223901 (2012)

[50] LookChem.com. Tin Bis(diethyldithiocarbamate). July 2013. <<http://www.lookchem.com/Tin-bis-diethyldithiocarbamate-/>>

[51] Y. C. Cheng, C. Q. Jin, F. Gao, et al. JOURNAL OF APPLIED PHYSICS 106, 123505 (2009)

[52] R. Abbel, T. van Lammeren, R. Hendriks. MRS Communications (2012), 2, 145–150

[53] D-H. KUO and T-R JAN. Journal of ELECTRONIC MATERIALS, Vol. 42, No. 6, 2013

[54] Fthenakis V., Morris S., Moskowitz P. and Morgan D., Toxicity of cadmium telluride, copper indium diselenide, and copper gallium diselenide, Progress in Photovoltaics, 7, 489-497, 1999.

[55] C-C. Kang, H-F Chen,T-C. Yu, et al. Materials Letters 96 (2013) 24–26